LLNL-JRNL-813628

Improvements to the macroscopic-microscopic approach of nuclear fission

Marc Verriere*
Theoretical Division, Los Alamos National Laboratory, Los Alamos, NM 87545, USA
Nuclear and Chemical Sciences Division, Lawrence Livermore National Laboratory, Livermore, California 94551, USA

Matthew Ryan Mumpower†
Theoretical Division, Los Alamos National Laboratory, Los Alamos, NM 87545, USA
(Dated: August 18, 2020)

The well established macroscopic-microscopic (mac-mic) description of nuclear fission enables the prediction of fission fragment yields for a broad range of fissioning systems. In this work, we present several key enhancements to this approach. We improve upon the microscopic sector of nuclear potential energy surfaces by magnifying the Lipkin-Nogami equations' resolution and strengthening the Strutinsky procedure, thus reducing spurious effects from the continuum. We further present a novel deterministic method for calculating fission dynamics under the assumption of strongly damped nucleonic motion. Our technique utilizes the memoryless property of Markov Chains to produce fission yields that do not rely on the statistical accumulation of scission events. We show that our new technique is equivalent to the Metropolis random-walk pioneered over the past decade by Randrup and colleagues. It further improves upon it, as we remove the need for altering the nuclear landscape via a biased potential. With our final improvement, we calculate scission configurations using particle number projection, which affords the simultaneous calculation of both mass and charge yield distributions. Fission fragments are thus calculated from the quantum mechanical A-body states of the potential energy surface rather than the collective mass asymmetry variable ($\alpha_{\rm g}$) of the Finite-Range Liquid-Drop Model (FRLDM) used in past work. We highlight the success of our enhancements by predicting the odd-even staggering and the charge polarization for the neutron-induced fission of ^{233}U and ^{235}U.

* verriere1@llnl.gov
† mumpower@lanl.gov

I. INTRODUCTION

The complexity of nuclear fission makes this reaction challenging to model theoretically from fundamental principles. Fission data, especially those based on fragment yields, are a key ingredient in many applications. For instance, the accurate description of fission yields is influential for nuclear engineering and waste management [1, 2], the production of radioactive isotopes via fragmentation [3–7], reactor neutrinos [8, 9], and in the pursuit of synthesizing superheavy elements [10–13]. Fission may also play an important role in the formation of the heavy elements in astrophysical processes [14–19].

There are many approaches to the theoretical description of fission. Fully microscopic models describe the fission process by assuming the nuclear interaction between the nucleons only. The most frequently used implementation is the Energy Density Functional (EDF) theory, where the density-dependence of the energy is derived from an effective interaction or directly parameterized. A quantum state is then extracted using a time-dependent mean-field approximation, such as the Time-Dependent Hartree-Fock method (TDHF), with the possibility to include dissipative effects [20–28] or through the resolution of the Schrödinger equation in a collective space defined with a reduced number of collective degrees of freedom (TDGCM), mainly the quadrupole and octupole multipolar moments [29–36]. The latter type of microscopic calculation can describe the fissioning system's deformations before scission only recently due to lengthy computational costs. Statistical methodologies also provide a practical path to obtain a description of fission and further enable large-scale calculations [37–39].

Approaching the description of fission observables from macroscopic-microscopic theory provides yet another alternative. In this approach, the fissioning system is modeled to first approximation as a macroscopic system (e.g., a liquid-drop or a droplet of nuclear matter) to obtain the smooth part of its energy [40, 41]. Corrections are then applied that account for the missing microscopic effects that may contribute to rapid variations in energy [42–44]. The time-evolution of the fissioning system is then obtained statistically with the exact or approximate resolution of the Langevin equations [45–47]. Approximate methods that assume strong damping are modeled via a random walk on the potential energy surface and are found to produce a good agreement with known data [48, 49].

The benefit of such semi-classical approaches over the microscopic approaches applied to the description of fission is the inclusion of larger spaces for the collective shape degrees of freedom and the ability to model stochastic dynamics, whilst retaining reasonable calculation times. Thus, such models are applicable to a range of reactions across many heavy fissioning systems [50]. To date, these approaches have examined several starting configurations for the dynamics, including from the ground state, inner saddle region, and after the last saddle [47, 50]. Those studies which start after the last saddle explicitly ignore dynamics before this point, potentially neglecting important pathways. Studies that start at the ground state may introduce a phenomenological tilting of the potential energy surface in an attempt to force the calculation to go over the fission barrier sufficiently quickly. The downside to the tilting is that it may introduce an unphysical bias to the results. Finally, the scission configurations of past work, e.g., [48], may be calculated with reference only to the collective asymmetry coordinate ($\alpha_{\rm g}$), thereby limiting the predictive power of the approach.

In this work, we address several of the major shortcomings of past macroscopic-microscopic fission studies to describe the nascent fission fragment yields. In Sec. II A, we outline the calculation of the potential energy surface, which has been improved by using an enhanced Strutinsky method that drastically reduces the continuum effects and allows the use of higher-quality particle basis. We present a new deterministic method to approximate fission dynamics in Sec. II B and show that it has the capacity to reproduce the results of past random-walk methods. Our new method has comparable calculation time while avoiding the use of biasing the potential energy surface. Further, we improve the estimation of the fission fragment mass and charge probability distribution based on a microscopic projection technique [51, 52]. In Sec. III, we present the results we have obtained with our approach.

II. THEORETICAL APPROACH

Our description of the fission process can be decomposed into three main steps. First, the shape-dependent potential energy surface (PES) of the corresponding fissioning system (typically target-plus-neutron) is determined using a semi-classical method based on the macroscopic Finite-Range Liquid-Drop Model (FRLDM) with microscopic corrections. An effective ground state and barrier height are then extracted from the PES, as presented in Sec. II A. In Sec. II B, we discuss our new Random-Walk-based algorithm used to obtain the probability to populate each scission configuration of the PES. Finally, in Sec. II C, we present how we can deduce, for the first time in this type of approach, the fission fragment probability distribution in charge and mass, $Y(Z, A)$, based on a microscopic projection technique.

A. Potential energy landscape

Several parameterizations of the sharp macroscopic density have been developed, see e.g., Ref. [53], to specify the relevant degrees of freedom associated with large deformations encountered in fission. In this work, we restrict ourselves to the description of binary fission. Even though there is experimental evidence for ternary [54–57] and even quaternary [58] fission, their contribution to the fragment probability distribution is smaller than binary fission by orders of magnitude. Thus, we use the so-called Matched-Quadratic-Surface (MQS) parameterization that was introduced in Refs. [59–62] for the specification of our shape families. The MQS parameterization contains nine degrees of freedom. Six degrees of freedom remain by ensuring a smooth junction between the bodies. Because one of the parameters corresponds to the center of mass, this may be set to the origin, reducing the number of parameters to five. We use the symbol $\boldsymbol{q}$ to denote a specific MQS shape. The lattice we use to calculate the PES is taken from Ref. [63]. We note that the nodes associated with $\alpha_g = -0.02$ are redundant due to parity-reversal symmetry, and therefore are not explicitly calculated.

For a nuclear system defined by Z protons, and N neutrons, the potential energy $E(\boldsymbol{q})$ associated with a given set of MQS parameters can be written as

$$E(\boldsymbol{q}) = E_{\rm mac}(\boldsymbol{q}) + \Delta E_{\rm shell}(\boldsymbol{q}) + \Delta E_{\rm pair.}(\boldsymbol{q}), \tag{1}$$

where $E_{\rm mac}(\boldsymbol{q})$ is the macroscopic energy, and the remaining terms define the microscopic corrections. It is obtained assuming that the fissioning system is a nuclear drop of charged liquid. Implicitly, these terms also depend on Z and N as discussed in greater detail in Appendix A.

In order to obtain the sharp contribution to the energy from shell effects, we determine a microscopic many-body state at the mean-field approximation. The effective averaged potential for the isospin τ is

$$V^{(\tau)}(\boldsymbol{q}) = V_1^{(\tau)}(\boldsymbol{q}) + V_{\rm C}^{(\tau)}(\boldsymbol{q}) + V_{\rm s.o.}^{(\tau)}(\boldsymbol{q}), \tag{2}$$

where each term is taken from Ref. [62]. The first term, $V_1^{(\tau)}$, corresponds to the parameterized mean-field associated with the central part of the nuclear interaction and is obtained assuming a Yukawa interaction between the nucleons,

$$V_1^{(\tau)}(\boldsymbol{r};\boldsymbol{q}) = -\frac{V_\tau}{4\pi a_{\rm pot}^3}\int_{\rm V} {\rm d}\boldsymbol{r}'\,\frac{e^{-|\boldsymbol{r}-\boldsymbol{r}'|/a_{\rm pot}}}{|\boldsymbol{r}-\boldsymbol{r}'|/a_{\rm pot}}, \tag{3}$$

where V is the shape associated with the MQS parameters, $\boldsymbol{q}$, scaled to have fixed volume, $\frac{4}{3}\pi A R_{\rm pot}^3$ ($R_{\rm pot}$ is defined by Eq. (81) of Ref. [64]). The potential depths V_τ are given by

$$V_{\rm n} = V_{\rm s} + V_{\rm a}\bar{\delta} \tag{4}$$

$$V_{\rm p} = V_{\rm s} - V_{\rm a}\bar{\delta}, \tag{5}$$

where $V_{\rm s}$ and $V_{\rm a}$ are parameters of the model and $\bar{\delta}$ is given by Eq. (85) of Ref. [64]. The Coulomb term $V_{\rm C}^{(\tau)}(\boldsymbol{r};\boldsymbol{q})$ is only acting on protons and given by

$$V_{\rm C}^{({\rm p})}(\boldsymbol{r};\boldsymbol{q}) = \frac{e^2 Z}{\frac{4}{3}\pi A r_0^2}\int_{\rm V}\frac{{\rm d}\boldsymbol{r}}{|\boldsymbol{r}-\boldsymbol{r}'|}. \tag{6}$$

The spin-orbit term has the expression

$$V_{\rm s.o.}^{(\tau)} = \lambda_\tau\left(\frac{\hbar^2}{2m_{\rm nuc}c}\right)^2\frac{\nabla V_1^{(\tau)}\boldsymbol{\sigma}\times\boldsymbol{p}}{\hbar} \tag{7}$$

where the interaction strength λ_τ is taken for each isospin τ as a linear function of the mass A [64] such that

$$\lambda_\tau = k_\tau A + l_\tau\ , \tag{8}$$

and k_τ and l_τ are parameters.

Assuming that the particles of the compound system are independent, the many-body state can, therefore, be obtained as a Slater determinant of particles, the state of each particle being an eigenfunction of the Hamiltonian associated with the energy e_i of the particle. Differentiating ourselves from past FRLDM work, the shell correction is calculated independently for each isospin by using the improved Strutinsky method presented in Ref. [65, 66]. This procedure removes spurious contribution from the continuum, which happens when the number of shells in

the Harmonic Oscillator basis, N_0, is set too large, thus causing divergences in the calculation of the energy. The avoidance of such spurious contributions is the reason why the size of the particle basis was limited to $N_0 = 12$ in past work. In this work, we use $N_0 = 20$, which is sufficiently larger than $N_0 = 12$ while remaining computationally manageable. We have tested our Strutinksy procedure up to $N_0 = 30$ and found no anomalies.

Pairing correlations are obtained using the Lipkin-Nogami approach with the seniority-pairing approximation on the Slater-determinant of particles used to estimate shell effects [67, 68]. The relevant equations read

$$N_{\text{pair}} = L_{\min} + \sum_{k=L_{\min}}^{L_{\max}} v_k^2 \tag{9}$$

$$\frac{2}{G} = \sum_{k=L_{\min}}^{L_{\max}} \frac{1}{\sqrt{(\epsilon_k - \lambda)^2 + \Delta^2}} \tag{10}$$

$$v_k^2 = \frac{1}{2}\left[1 - \frac{\epsilon_k - \lambda}{\sqrt{(\epsilon_k - \lambda)^2 + \Delta^2}}\right] \tag{11}$$

$$\epsilon_k = e_k + (4\lambda_2 - G)v_k^2 \tag{12}$$

$$\lambda_2 = \frac{G}{4}\left\{\frac{\displaystyle\sum_{k=L_{\min}}^{L_{\max}} u_k^3 v_k \sum_{\substack{l=L_{\min} \\ l\neq k}}^{L_{\max}} u_l v_l^3}{\displaystyle\sum_{k=L_{\min}}^{L_{\max}} u_k^2 v_k^2 \sum_{\substack{l=L_{\min} \\ l\neq k}}^{L_{\max}} u_l^2 v_l^2}\right\}. \tag{13}$$

This is a nonlinear system of $2N_{\text{v}} + 3$ equations, where $N_{\text{v}} = L_{\max} - L_{\min} + 1$ is the number of pairs in the valence space. The unknowns of this systems are the pairing gap Δ, the Fermi energy λ, the number-fluctuation constant λ_2 and for $k = L_{\min} \dots L_{\max}$, v_k are the occupation amplitudes and ϵ_k are the shifted single-particle energies. This system of equations is completely determined by the single-particle energies e_k, the number of paired levels N_{pair}, the first and last levels $0 \leq L_{\min} \leq L_{\max}$ in the valence space and the seniority-pairing strength, G. The latter is obtained using a method based on Ref. [69]. Specifically, to obtain an expression for G, we assume that the spacing between the energy levels is constant

$$\epsilon_k - \tilde{\lambda} = \frac{k - N_{\text{pair}}}{\tilde{\rho}}. \tag{14}$$

In this expression, $\tilde{\lambda}$ is the smooth Fermi energy of the smoothed single-particle energy and $\tilde{g}$ is the smooth level density obtained with the Strutinsky method. The pairing gap Δ in (11) is approximated by an effective pairing gap

$$\bar{\Delta} = \begin{cases} \frac{r_{\text{mic}} B_s}{N^{1/3}} & \text{for neutrons} \\ \frac{r_{\text{mic}} B_s}{Z^{1/3}} & \text{for protons} \end{cases}. \tag{15}$$

We then substitute the sum of (11) by an integral

$$\sum_{k=L_{\min}}^{L_{\max}} f(\epsilon_k - \lambda) \approx \tilde{\rho} \int_{y_1}^{y_2} f(x)\,\mathrm{d}x \tag{16}$$

to obtain the following expression for G

$$G = \frac{2}{\tilde{\rho}}\left[\operatorname{arsinh}\left(\frac{y_2}{\bar{\Delta}}\right) - \operatorname{arsinh}\left(\frac{y_1}{\bar{\Delta}}\right)\right]^{-1}, \tag{17}$$

where

$$y_1 = \frac{L_{\min} - N_{\text{pair}} - \frac{1}{2}}{\tilde{\rho}} \tag{18}$$

$$y_2 = \frac{L_{\max} - N_{\text{pair}} + \frac{1}{2}}{\tilde{\rho}}. \tag{19}$$

Note that these expressions differ from the one obtained in [41, 64], being shifted by $1/(2\tilde{\rho})$. The expression of the average pairing correlation plus quasi-particle energy $\tilde{E}_{\text{p.c.}}$ is then obtained by inserting these quantities into Eq. (110) of Ref. [64].

We solve the Lipkin-Nogami equations (9)-(13) using a new method based on the analytical calculation of the full Lipkin-Nogami Jacobian and the action of its inverse on any vector coupled with a fifth-order numerical scheme. We set multiple starting points to avoid local minima and find that our method greatly enhances the success rate of the resolution of the Lipkin-Nogami equations. Thus, the time required to solve the Lipkin-Nogami equations using our method is faster than in older work. This means the calculation time for our procedure is now negligible compared to the calculation and diagonalization time of the Hamiltonian, thus allowing for larger shape families or potential energy surfaces to be explored in the future. This new method is described in detail in Appendix B.

B. Novel approach to strongly damped nuclear motion

Many different methods have been developed to calculate nascent fission fragment yields. Most of these methods seek to simplify the time-evolution of the complex nuclear motion subject to various assumptions, see Ref. [50] for a recent overview. One of the most successful methods pursued over the past ten years is the assumption of strongly damped nuclear dynamics in which the Smoluchowski equations reduce to a Metropolis random walk (RW) [48, 70]. This method has been used in a large range of fission reactions using Markov Chain Monte Carlo (MCMC) sampling [49, 50, 71–73]. The primary drawback to this method is the long calculation time required for near-barrier fission. In what follows, we briefly review the construction of the finite-temperature PES and the MCMC sampling method. We then present our new Deterministic-Probabilistic Algorithm (DPA) for attaining scission configurations under the assumption of strongly damped motion.

The finite-temperature potential energy $U(\boldsymbol{q})$ for each points of the PES is obtained through the insertion of a suppression factor $\mathcal{S}[E^*(\boldsymbol{q})]$ in Eq. (1),

$$U(\boldsymbol{q}) = E_{\text{mac}}(\boldsymbol{q}) + \mathcal{S}[E^*(\boldsymbol{q})]\Delta E_{\text{s+p}}(\boldsymbol{q}) \tag{20}$$

$$\Delta E_{\text{s+p}}(\boldsymbol{q}) = \Delta E_{\text{shell}}(\boldsymbol{q}) + \Delta E_{\text{pair.}}(\boldsymbol{q}) \tag{21}$$

$$\mathcal{S}[E^*] = \frac{1+\exp(-E_1/E_0)}{1+\exp((E^*-E_1)/E_0)}\ , \tag{22}$$

where $E^*(\boldsymbol{q}) = E^* - E(\boldsymbol{q})$ is the local excitation energy as in Ref. [49]. A discrete or continuous Random-Walk (RW) is then used on the finite-temperature PES $U(\boldsymbol{q})$ to ascertain the scission configurations for the given incident energy, E^*.

The MCMC RW procedure is illustrated in Fig. 1a. A single step can be decomposed as follows:

1. start at an initial point $\boldsymbol{q}_0$ (state $\mathcal{P}_0$);
2. randomly choose one of its D neighbors $\boldsymbol{q}_k$ ($k = 1, \ldots, D$) using a uniform distribution (transition from $\mathcal{P}_0$ to one of the $\mathcal{I}_k$);
3. if
   (a) $U(\boldsymbol{q}_k) \leq U(\boldsymbol{q}_0)$, then,

$$\mathbb{P}^{\text{acc.}}_{0\to k} = 1 \qquad \mathbb{P}^{\text{rej.}}_{0\to k} = 0 \tag{23}$$

   where $\mathbb{P}^{\text{acc.}}_{0\to k}$ is the acceptance probability and $\mathbb{P}^{\text{rej.}}_{0\to k}$ is the rejection probability. We accept $\boldsymbol{q}_k$ as a the next point (transition from state $\mathcal{I}_k$ to another state $\mathcal{P}_k$);

   (b) $U(\boldsymbol{q}_k) > U(\boldsymbol{q}_0)$, then, we sample a random variable $r \sim U([0,1])$. If $r < \mathbb{P}^{\text{rej.}}_{0\to k} = 1 - \mathbb{P}^{\text{acc.}}_{0\to k}$, where

$$\mathbb{P}^{\text{acc.}}_{0\to k} = \exp\left(-\frac{U(\boldsymbol{q}_k) - U(\boldsymbol{q}_0)}{T}\right)\ , \tag{24}$$

   then go back to $\boldsymbol{q}_0$ (transition from $\mathcal{I}_k$ to $\mathcal{P}_0$). Otherwise, accept $\boldsymbol{q}_k$ as the next point (transition from $\mathcal{I}_k$ to $\mathcal{P}_k$).

Results using this approach are always obtained through the generation of paths by explicitly repeating these steps from an initial point up to reaching a scission shape. A scission shape is defined such that the radius of its neck, if

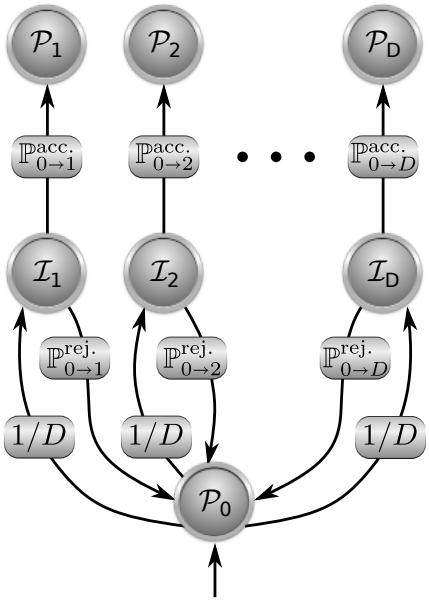

(a) Graph of the Markov-Chain transitions associated with the Random-Walk method.

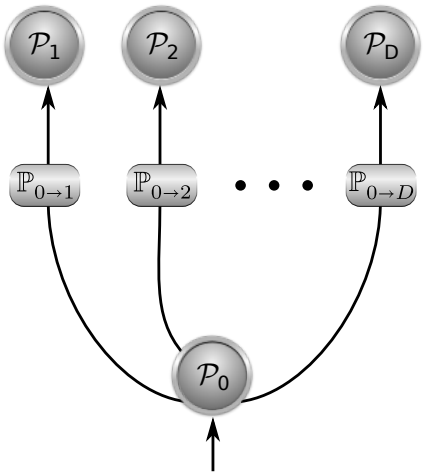

(b) Loop-less graph of the Markov Chain transitions of the Markov-Chain associated with the Random-Walk method.

present, is lower than a given parameter r_{neck}. Many paths have to be calculated to reduce the statistical uncertainty and obtain a reasonable estimation of the probability density function (PDF) for the scission configurations.

We propose here to directly determine the evolution of the PDF according to the number of steps in a path. This transformation is analogous to the determination of the Fokker-Plank equations associated with the Langevin equations. The first step is to unravel the loops $\mathcal{P}_0 \to \mathcal{I}_k \to \mathcal{P}_0$ appearing in Fig. 1a. This can be visualized by the transition graph of Fig. 1b.

The probabilities $\mathbb{P}_{0\to k}$ to reach $\mathcal{P}_k$ from $\mathcal{P}_0$ is the sum of the probabilities of all possible paths between $\mathcal{P}_0$ and $\mathcal{P}_k$. Such a path can be decomposed into two parts: the first one is the self-looping from $\mathcal{P}_0$ to $\mathcal{P}_0$ and the second one is $\mathcal{P}_0 \to \mathcal{I}_k \to \mathcal{P}_k$ and corresponds to the last two transitions of the path. Using the Markov property of *memoryless* transitions, the probability $\mathbb{P}_{0\to k}$ to reach $\mathcal{P}_k$ from $\mathcal{P}_0$ through any path can be decomposed as the product of the probability C to reach $\mathcal{P}_0$ starting from $\mathcal{P}_0$ which is independent of k and the probability to reach $\mathcal{P}_k$ from $\mathcal{P}_0$ without going around any loop

$$\mathbb{P}_{0\to k} = C \times \frac{\mathbb{P}^{acc.}_{0\to k}}{D} \ . \tag{25}$$

and D is the enumeration of states directly connected with $\mathcal{P}_0$. Using again the memoryless transitions property, it can be shown that the probability to reach $\mathcal{P}_0$ after $2N$ iterations is

$$\mathbb{P}^{(2N)}_{0\to0} = \left[\sum_{k=1}^{D} \frac{\mathbb{P}^{rej.}_{0\to k}}{D}\right]^N \ , \tag{26}$$

which goes to zero as N goes to infinity. Therefore, we have

$$\sum_{k=1}^{D} \mathbb{P}_{0\to k} = C \times \sum_{k=1}^{D} \frac{\mathbb{P}^{acc.}_{0\to k}}{D} = 1 \ . \tag{27}$$

This relation enables the calculation of C without resorting to its definition as an infinite sum to obtain

$$C = \frac{D}{\sum_{k=1}^{D} \mathbb{P}^{acc.}_{0\to k}} \ , \tag{28}$$

leading to

$$\mathbb{P}_{0\to k} = \frac{\mathbb{P}^{\text{acc.}}_{0\to k}}{\sum_{k=1}^{D} \mathbb{P}^{\text{acc.}}_{0\to k}} \ . \tag{29}$$

Note that these formulas can also be derived by directly using the definition of C

$$C \equiv \sum_{N=0}^{\infty} \mathbb{P}^{(2N)}_{0\to 0} = \frac{1}{\sum_{k=1}^{D} \frac{\mathbb{P}^{\text{acc.}}_{0\to k}}{D}} \ , \tag{30}$$

where Eq. (26), the Taylor series of the function $x \mapsto 1/(1-x)$ and the relation $\mathbb{P}^{\text{rej.}}_{0\to k} = 1 - \mathbb{P}^{\text{acc.}}_{0\to k}$ have been used. The corresponding transition probabilities from a point $\boldsymbol{q}_0$ to $\boldsymbol{q}_k$ are thus proportional to $\mathbb{P}^{\text{acc.}}_{0\to k}$. Our derivation shows that in the standard RW method, there exists a parameter that correspond to an energy threshold, $\Delta U_{\text{thresh.}} = 0$ MeV, on the energy difference, $U(\boldsymbol{q}_k) - U(\boldsymbol{q}_0)$, below which a transition from $\mathcal{I}_k$ to $\mathcal{P}_k$ is certain to happen (with probability 1).

With the probability of an individual step well defined, we now seek to calculate the probability distribution after a fixed number of RW steps. This quantity, $p^{(n+1)}_{\mathcal{R}}(\boldsymbol{q}_{\text{f}})$, is defined as the probability distribution associated with the random variable $\mathcal{R}_{n+1}$ to reach a point, $\boldsymbol{q}_{\text{f}}$, after $n+1$ RW steps and can be obtained recursively from the distribution $p^{(n)}_{\mathcal{R}}$ after n steps using

$$p^{(n+1)}_{\mathcal{R}}(\boldsymbol{q}_{\text{f}}) = \sum_{\boldsymbol{q}} \mathbb{P}^{\text{acc.}}_{\boldsymbol{q}\to\boldsymbol{q}_{\text{f}}} p^{(n)}_{\mathcal{R}}(\boldsymbol{q}) \ . \tag{31}$$

From this definition it is clear that the probability distribution after n steps is thus completely determined by the choice of the initial probability distribution $p^{(0)}_{\mathcal{R}}$.

Rather than using Eq. (31) to directly compute our scission PDF, we generalize our procedure by allowing a distribution of ending configurations. This amounts to adding an absorption mechanism on top of the nuclear PES, analogous to the idea introduced in Ref. [30]. At each step n of our calculation we add an absorption field $A(\boldsymbol{q})$ such that

$$\bar{a}^{(n)}_{\mathcal{R}}(\boldsymbol{q}) = \bar{a}^{(n-1)}_{\mathcal{R}} + A(\boldsymbol{q}) p^{(n)}_{\mathcal{R}}(\boldsymbol{q}) \tag{32}$$

$$a^{(n)}_{\mathcal{R}}(\boldsymbol{q}) = \frac{\bar{a}^{(n)}_{\mathcal{R}}(\boldsymbol{q})}{\sum_{\boldsymbol{q}'} \bar{a}^{(n)}_{\mathcal{R}}(\boldsymbol{q}')} \tag{33}$$

where $\boldsymbol{q}$ and $\boldsymbol{q}'$ are two distinct shape configurations, $\bar{a}^{(n)}_{\mathcal{R}}$ is the probability to reach a given shape at a given iteration, $a^{(n)}_{\mathcal{R}}(\boldsymbol{q})$ is the probability to reach a shape $\boldsymbol{q}$ after n iterations given that $\boldsymbol{q}$ is a scission shape. We let $\bar{a}^{(0)}_{\mathcal{R}}(\boldsymbol{q}) = 0$ and the values of the absorption field $0 \leq A(\boldsymbol{q}) \leq 1$ correspond to the percentage of the probability distribution absorbed after one step at $\boldsymbol{q}$. The Eq. (31) is then replaced by

$$p^{(n+1)}_{\mathcal{R}}(\boldsymbol{q}_{\text{f}}) = \sum_{\boldsymbol{q}} \mathbb{P}^{\text{acc.}}_{\boldsymbol{q}\to\boldsymbol{q}_{\text{f}}} \bar{p}^{(n)}_{\mathcal{R}}(\boldsymbol{q}) \ . \tag{34}$$

where the initial probability distribution at the next iteration $\bar{p}^{(n)}_{\mathcal{R}}(\boldsymbol{q})$ is then taken to be

$$\bar{p}^{(n)}_{\mathcal{R}}(\boldsymbol{q}) = (1 - A(\boldsymbol{q})) p^{(n)}_{\mathcal{R}}(\boldsymbol{q}) \ . \tag{35}$$

In this first work, we set the absorption field, $A(\boldsymbol{q})$, to 100% for scission configurations and zero otherwise. This allows us to directly compare to previous work in the Section III. The absorption field can in principle be configured in any number of ways, including a distribution for various neck sizes, instead of the implicitly assumed sharp function of this work. We plan to study such possibilities in future work.

Our novel method also affords the calculation of a convergence criteria. We can use this quantity as an estimate of the statistical uncertainty on calculated fission yields. To this end, we assume that the 1-distance (the distance associated with the 1-norm $||.||_1$) between two distributions $a^{(n)}_{\mathcal{R}}$ and $a^{(n+j)}_{\mathcal{R}}$, defined as

$$\Delta^{(n)}_{(j)} = \sum_{\boldsymbol{q}} \left| a^{(n+j)}_{\mathcal{R}}(\boldsymbol{q}) - a^{(n)}_{\mathcal{R}}(\boldsymbol{q}) \right| , \tag{36}$$

is an inverse-quadratic function

$$\Delta_{(j)}^{(n)} \approx \frac{1}{[c(j)n + d(j)]^2} \ , \tag{37}$$

where j is an integer, $c(j)$ and $d(j)$ are two real parameters that are ultimately obtained using a fit procedure. The validity of this assumption is discussed in III for $j = 1000$. The convergence error at a step n can be introduced as the distance between the distribution at step n and the distribution at infinity

$$\varepsilon^{(n)} = \Delta_{(\infty)}^{(n)}. \tag{38}$$

Using the subadditivity of the 1-distance (commonly referred as the triangle inequality), we can determine the convergence criteria,

$$\varepsilon^{(n)} \leq \sum_{k=0}^{\infty} \Delta_{(j)}^{(n+kj)} \ . \tag{39}$$

Inserting (37) into (39) gives

$$\varepsilon^{(n)} \leq \sum_{k=0}^{\infty} \frac{1}{\left[(jc(j))k + (c(j)n + d(j))\right]^2} \ . \tag{40}$$

A closed form of the right-hand side of this expression can be obtained by resorting to the trigamma function defined as

$$\phi^{(1)}(z) = \frac{\mathrm{d}^2}{\mathrm{d}z^2} \ln \Gamma(z) \ , \tag{41}$$

that satisfies

$$\phi^{(1)}(z) = \sum_{k=0}^{\infty} \frac{1}{(k+z)^2} \ . \tag{42}$$

Employing these properties of the trigamma function, we finally obtain

$$\varepsilon^{(n)} \leq \varepsilon_{\text{eff.}}^{(n,j)} \ , \tag{43}$$

where

$$\varepsilon_{\text{eff.}}^{(n,j)} = \frac{1}{[jc(j)]^2} \phi^{(1)} \left(\frac{c(j)n + d(j)}{jc(j)} \right) \ . \tag{44}$$

We take $\varepsilon_{\text{eff.}}^{(n,j)}$ as our convergence criteria as it is an upper limit on the error $\varepsilon^{(n)}$ after n iterations.

C. Mass and charge yields of fission fragments

Most of the current mac-mic models used to estimate the probability distribution associated with the fission fragment properties before prompt emissions resort to obtaining the mass, $Y(A_\mathrm{f})$, or charge, $Y(Z_\mathrm{f})$, yields separately using the relevant macroscopic shape parameter, e.g., the procedure of Ref. [72]. While this method has been highly successful, see e.g. [48, 70], it does not provide a means to calculate the full fragment yield, $Y(Z_\mathrm{f}, A_\mathrm{f})$ or equivalently, $Y(Z_\mathrm{f}, N_\mathrm{f})$. In the past, the full mass and charge yields have obtained through the direct analysis of systematics on known experimental data [74], thus with low predictive power albeit high-quality data, or using the Wahl systematics [75] e.g., in Ref. [50], which introduces a free parameter σ_Z that controls the dispersion in charge of the isobaric yields, and presumes the Unchanged Charge Distribution (UCD) assumption that relies on the ratio $\eta \equiv \frac{Z_\mathrm{f}}{A_\mathrm{f}} = \frac{Z}{A}$. Another method, presented in Ref. [76], aims at obtaining the full mass and charge yields but relies on the addition of a sixth macroscopic shape parameter in the PES. Without adding specific parameters, none of these past approaches can predict the fission fragments' charge polarization, which is the experimentally observed deviation from the UCD assumption.

In the following, we construct an approach to predict the full probability distribution of the fission fragment mass *and* charge $Y(Z_\mathrm{f}, A_\mathrm{f})$ directly from the quantum mechanical wavefunctions. As it will be shown in Sec. III A, our projection technique is able to reproduce charge polarization and odd-even staggering in the fragments without additional parameters.

We only consider here the nascent fragments in binary fission. Therefore, $Y(Z_\mathrm{f}, A_\mathrm{f})$ can be decomposed according to the probability distribution, $Y_\mathrm{L}(Z_\mathrm{f}, A_\mathrm{f})$, (normalized to 1) associated with the mass and charge of only the left fragment,

$$Y(Z_\mathrm{f}, A_\mathrm{f}) = Y_\mathrm{L}(Z_\mathrm{f}, A_\mathrm{f}) + Y_\mathrm{L}(Z - Z_\mathrm{f}, A - A_\mathrm{f}) \ . \tag{45}$$

The law of total probability enables the decomposition of the probability distribution of the number of particles in the left fragment $Y_\mathrm{L}(Z_\mathrm{f}, A_\mathrm{f})$ before prompt particle emission as follows,

$$Y_\mathrm{L}(Z_\mathrm{f}, A_\mathrm{f}) = \int \mathbb{P}\left((Z, A)_\mathrm{L} = (Z_\mathrm{f}, A_\mathrm{f}) \,|\, \mathcal{R} = \boldsymbol{q}\right) a_\mathcal{R}(\boldsymbol{q})^{(\infty)} \,\mathrm{d}\boldsymbol{q} \ , \tag{46}$$

where the integral iterates over all the scission shapes parameterized by $\boldsymbol{q}$, $a_\mathcal{R}^{(\infty)}(\boldsymbol{q})$ is the limit for $n \to \infty$ of the distributions introduced in Eq. (33) and $\mathbb{P}\left((Z, A)_\mathrm{L} = (Z_\mathrm{f}, A_\mathrm{f}) \,|\, \mathcal{R} = \boldsymbol{q}\right)$ is the probability associated with a left fragment of mass A_f and charge Z_f when the fissioning system is in the shape $\boldsymbol{q}$. Note that to use the law of total probability, we had to implicitly assume that there *exists* a set of random variables $\mathcal{R}_0, \ldots, \mathcal{R}_\infty$, as in the previous section. It is not always the case, such as in the Time-Dependent Generator Coordinate Method formalism [77]. In this case, coupling terms have to be added in the decomposition of $Y_\mathrm{L}(Z_\mathrm{f}, A_\mathrm{f})$.

The probability $\mathbb{P}\left((Z, A)_\mathrm{L} = (Z_\mathrm{f}, A_\mathrm{f}) \,|\, \mathcal{R} = \boldsymbol{q}\right)$ is extracted from the microscopic state calculated to estimate the shell+pairing correction for each coordinate $\boldsymbol{q}$ of the PES after projection on the good mass and charge of the total fissioning system. Because all these states preserve the isospin, we can further decompose

$$\mathbb{P}\left((Z, A)_\mathrm{L} = (Z_\mathrm{f}, A_\mathrm{f}) \,|\, \mathcal{R} = \boldsymbol{q}\right) = \mathbb{P}\left(N_\mathrm{L} = N_\mathrm{f} \,|\, \mathcal{R} = \boldsymbol{q}\right) \mathbb{P}\left(Z_\mathrm{L} = Z_\mathrm{f} \,|\, \mathcal{R} = \boldsymbol{q}\right), \tag{47}$$

where N_f is the number of neutrons in the left fragment. Both factors in the right-hand side of Eq. (47) are calculated through the particle-number projection-based technique on the fragments mass and charge developed first in Ref. [51] in the context of time-dependent mean-field calculations for transfer reactions. This technique was first applied to fission in Ref. [78] and adapted to the case of static mean-field calculations in Ref. [52]. When applied to fission, this technique gives the probabilities associated with the number of nascent fragment neutrons ($X = N$, $X_\mathrm{f} = N_\mathrm{f}$) and protons ($X = Z$, $X_\mathrm{f} = Z_\mathrm{f}$) using,

$$\mathbb{P}\left(X_\mathrm{L} = X_\mathrm{f} \,|\, \mathcal{R} = \boldsymbol{q}\right) = \frac{\left\langle \Phi(\boldsymbol{q}) \middle| \hat{P}_{X_\mathrm{f}}^{(L)} \hat{P}_X \middle| \Phi(\boldsymbol{q}) \right\rangle}{\left\langle \Phi(\boldsymbol{q}) \middle| \hat{P}_X \middle| \Phi(\boldsymbol{q}) \right\rangle}, \tag{48}$$

or equivalently

$$\mathbb{P}\left(X_\mathrm{L} = X_\mathrm{f} \,|\, \mathcal{R} = \boldsymbol{q}\right) = \frac{\left\langle \Phi(\boldsymbol{q}) \middle| \hat{P}_{X_\mathrm{f}}^{(L)} \hat{P}_X^{(R)} \middle| \Phi(\boldsymbol{q}) \right\rangle}{\left\langle \Phi(\boldsymbol{q}) \middle| \hat{P}_X \middle| \Phi(\boldsymbol{q}) \right\rangle}. \tag{49}$$

A double projection is required, where $\hat{P}_{X=N,Z}$ is the operator restoring the good number of particle in the total system while $\hat{P}_{X_\mathrm{f}}^{(L)}$ is an operator projecting on X_f particles in the left fragment. The definition of the latter relies on the position of the neck along the symmetry axis. We define this quantity, in the standard way, as the position of the minimum of the local one-body density of the microscopic state in $\boldsymbol{q}$ between the two pre-fragments [34, 79, 80]. The projection-based method to calculate the fragment distribution is already known to describe the odd-even staggering of the charge distribution of the fragments in case of time-dependent mean-field methods [78] and is able to give non-zero probability for the existence of fragments with odd-number of particles [52]. At first sight, it could seem to be a paradox in the case of static mean-field calculations in the case of even-even systems since:

1. the state describing the fissioning system is time-even;
2. the operators $\hat{P}_X$ and $\hat{P}_{X_\mathrm{f}}^{(L)}$ are time-even;
3. a state describing odd-number fragments cannot be time-even.

However, this paradox is only apparent and can be solved by noticing that the projection operators are both acting on the full X-body wavefunction (for each isospin). Even in the case where X_f is odd, the state $\hat{P}^{(L)}_{X_\mathrm{f}}\hat{P}_X\left|\Phi(\boldsymbol{q})\right\rangle$ contains an even number of particles: X_f in the left fragment and $X - X_\mathrm{f}$ in the right one. It is thus time-even. It can easily be seen from a simple example of a time-even state having only two particles

$$\left|\Phi\right\rangle = \hat{a}^\dagger_i\hat{a}^\dagger_{\bar{i}}\left|0\right\rangle, \tag{50}$$

where $\hat{a}^\dagger_i$ is the creation operator of a particle in state i, $\bar{i}$ is the time-reveral state of i. Both states can be decomposed in a similar way as in [51, 52] as

$$\hat{a}^\dagger_i = \alpha^{(L)}_i\hat{a}^{(L)\dagger}_i + \alpha^{(R)}_i\hat{a}^{(R)\dagger}_i \tag{51}$$

$$\hat{a}^\dagger_{\bar{i}} = \alpha^{(L)\star}_i\hat{a}^{(L)\dagger}_{\bar{i}} + \alpha^{(R)\star}_i\hat{a}^{(R)\dagger}_{\bar{i}}, \tag{52}$$

where $\hat{a}^{(L)\dagger}_k$ and $\hat{a}^{(R)\dagger}_k$ are respectively the left and right parts of $\hat{a}^\dagger_k$ for $k = i, \bar{i}$. The creation operators on the left commute with the ones on the right due to the complete separation of their spatial domain, and each of them commute with their time-reversal. Therefore, by injecting (51) and (52) into (50) and developing the resulting expression, we obtain

$$\begin{aligned}\left|\Phi\right\rangle = \alpha^{(L)}_i\alpha^{(L)\star}_i\hat{a}^{(L)\dagger}_i\hat{a}^{(L)\dagger}_{\bar{i}}\left|0\right\rangle + \\ \left(\alpha^{(L)}_i\alpha^{(R)\star}_i\hat{a}^{(L)\dagger}_i\hat{a}^{(R)\dagger}_{\bar{i}} + \alpha^{(R)}_i\alpha^{(L)\star}_i\hat{a}^{(R)\dagger}_i\hat{a}^{(L)\dagger}_{\bar{i}}\right)\left|0\right\rangle + \\ \alpha^{(R)}_i\alpha^{(R)\star}_i\hat{a}^{(R)\dagger}_i\hat{a}^{(R)\dagger}_{\bar{i}}\left|0\right\rangle.\end{aligned} \tag{53}$$

The three terms are orthogonal to each other and are all time-even. The first one corresponds to a state with two particles in the left side and zero in the right one, the second one corresponds to one particle on each side and the last one corresponds to two particles in the right side and zero in the left one. Therefore, even though $\left|\Phi\right\rangle$ is time-even and $\hat{P}^{(L)}_1$ is time-even, we have a non-zero probability to have odd-number fragments when the state i spreads on both the left and right domains

$$\mathbb{P}\left(X_\mathrm{L} = X_\mathrm{f}\right) = \frac{\left\langle\Phi\right|\hat{P}^{(L)}_{X_\mathrm{f}}\left|\Phi\right\rangle}{\left\langle\Phi|\Phi\right\rangle} = 2|\alpha^{(L)}_i\alpha^{(R)}_i|^2. \tag{54}$$

However, as shown and explained in Ref. [52] in the case of static time-even Bogoliubov states with an even-number of particles, the probability associated with odd-number fragments collapse to zero as soon as the fragments are separated enough and don't interact anymore. This is a direct consequence of the finite-range character of the nuclear interaction and the minimization of the energy: if two subsystems $\mathcal{S}_1$ and $\mathcal{S}_2$ of a system $\mathcal{S}$ do not interact with each other, the energy of the total system is the sum of the energies of both subsystems and thus, the state that minimize the energy of $\mathcal{S}$ is the product of the states minimizing each subsystems.

III. APPLICATION TO 233,235-U(N,F)

We illustrate our model improvements in what follows by showcasing the well-known neutron-induced fission of two isotopes of Uranium, ^{233,235}U(n,f). We also prove that our implementation can reproduce the results of the discrete random-walk method used in past work.

In Refs. [41, 63, 64, 71–73, 81], the authors implemented shell-plus-pairing corrections through the resolution of the Schrödinger equation using an Axial Harmonic Oscillator (AHO) basis with only $N_\mathrm{sh} = 12$ shells. The limitation of this previous approach artificially introduces spurious contributions of the continuum [66]. The use of the improved Strutinsky method [65] allows us to remove these contributions and thus use instead $N_\mathrm{sh} = 20$ shells without any energy truncation. In addition, we optimize the oscillator scaling factor b_0 and deformation q for each point of the PES using a variational principle such that the mean-field-plus-pairing energy of the microscopic state is minimized.

The order of the Strutinsky method is $p = 8$, and the corresponding range is

$$\gamma = C_\mathrm{sr}\frac{C_\mathrm{cur}}{A^{1/3}}B_\mathrm{s}, \tag{55}$$

where the relative surface energy $B_\mathrm{s}(\boldsymbol{q})$ is the ratio of the nucleus surface at shape $\boldsymbol{q}$ with the surface of the same nucleus at spherical shape. We have used the same parameters as in Ref. [64], listed in the following table.

Parameter	Value	Unit
$C_{\rm sr}$	1.0	MeV
$C_{\rm cur}$	41	MeV

TABLE I: Microscopic parameters associated with the Strutinsky correction.

The pairing correction is obtained using the Lipkin-Nogami method. We have solved the Lipkin-Nogami (LN) for each point of the PES using a pairing window of $\pm$ 5 MeV around the Fermi surface. The only remaining parameter is the LN effective-interaction pairing gap constant $r_{\rm mic} = 3.2$ MeV. The full LN equations are often numerically solved by splitting them into two or more subsets of equations, solved separately at each iteration. It adds overhead in the resolution time and can also lead to spurious divergences. Instead, we have developed a new method to solve these equations. Our method is based on the iterative fifth-order method presented in Ref. [82] that only requires first-order derivatives (i.e., the Jacobian matrix). The main steps of our method are presented in Appendix B.

The fragment probabilities at each $\boldsymbol{q}$ are calculated using Eq. (49). The double-projection on the numerator is calculated using the Pfaffian technique presented in Refs. [83, 84]. The determination of the integrals over the gauge angles are determined through a Fomenko discretization method [85]. For each scission shape, we find the optimal number of integration point $N_{\rm Fom.}$ by assuming that the width of the fragment distribution associated with both isospin is $N_{\rm Fom.}$. We check if this assumption is correct by checking that

$$\mathbb{P}\left(X_{\rm L} = X_{\rm f} \,|\, \mathcal{R} = \boldsymbol{q}\right) < 1.0 \times 10^{-6} \tag{56}$$

for all $X_{\rm f} = \lfloor X_{\rm mean} - N_{\rm Fom.}/2 \rfloor + \Delta X$ and $X_{\rm f} = \lceil X_{\rm mean} + N_{\rm Fom.}/2 \rceil - \Delta X$ for $\Delta X = 0, 1, 2$ and both isospins. If it is not the case, we add 10 integration points and test again our criteria up to finding the value of $N_{\rm Fom.}$ that satisfies it, starting at $N_{\rm Fom.} = 30$.

The PES at a given excitation energy is obtained through the finite temperature method of Ref. [49] where the damping of the shell-plus-pairing correction as in Eq. (20) invokes the damping parameter $\mathcal{S}[E^*]$ defined in Eq. (22). The two parameters we have taken to define the damping coefficient are $E_0 = 20$ MeV and $E_1 = 15$ MeV. The excitation energy dependency of the temperature is taken at the Thomas-Fermi approximation to be

$$E^*(\boldsymbol{q}) = aT(\boldsymbol{q})^2, \tag{57}$$

with the nuclear level density $a = A/8$. To obtain an implementation equivalent to the state-of-the-art random-walk, we have set $\Delta U_{\rm thresh.} = 0$ MeV. Recall that this threshold does not directly appear in the standard formalism of the random-walk and corresponds to the energy difference $U(\boldsymbol{q}_k) - U(\boldsymbol{q}_0)$ between an initial point $\boldsymbol{q}_0$ and one of its neighbor $\boldsymbol{q}_k$ below which a transition from the states $\mathcal{I}_k$ to $\mathcal{P}_k$ is certain in the Markov Chain Fig. 1a. The potential energy surface is calculated on a regular grid following the work of Ref. [63]. Two points $\boldsymbol{q}_0$ and $\boldsymbol{q}_1$ are neighbors if all the integer coordinates on the lattice differ by at most one unit. Such a definition in five dimensions leads to a maximum of $3^5 - 1 = 242$ neighbors for each node of the grid.

Our initial distribution is chosen to be entirely on the lattice site that corresponds to the effective ground-state of the PES. The determination of this point is obtained as follow:

1. we start at the origin of the lattice associated with the smallest elongation, a maximal neck radius, and spherical left and right bodies of the same volume;
2. we iterate over the neighbors of the points, we select the neighbor that is associated with the lowest energy, and we reiterate up to reaching a local minimum $\boldsymbol{q}_{\rm loc}$;
3. we determine the minimum energy $E_{\rm sad.}$ required to reach scission configurations from $\boldsymbol{q}_{\rm loc}$;
4. we calculate the set $\mathcal{C}$ of all the configurations accessible from $\boldsymbol{q}_{\rm loc}$ with an energy lower than $E_{\rm sad.}$, and define the effective ground-state as the node $\boldsymbol{q}_{\rm g.s.} \in \mathcal{C}$ associated with the lowest energy $E_{\rm g.s.}$.

By using this procedure, we also obtain the saddle energy $E_{\rm sad}$, as well as an effective barrier height $E_{\rm B} = E_{\rm sad} - E_{\rm g.s.}$. A site of the lattice is a scission configuration if its corresponding sharp macroscopic density has a neck radius $r_{\rm neck} < r_{\rm sciss.}$. We have calculated the fragment probability distribution for

$$r_{\rm sciss} = 1.75, 2.25, 2.75 \text{ fm} \tag{58}$$

and three different excitation energies E^* such that

$$x = E^* - E_{\rm B} = 0.1, 2.0, 4.0 \text{ MeV}, \tag{59}$$

for a total of nine fission calculations per nucleus.

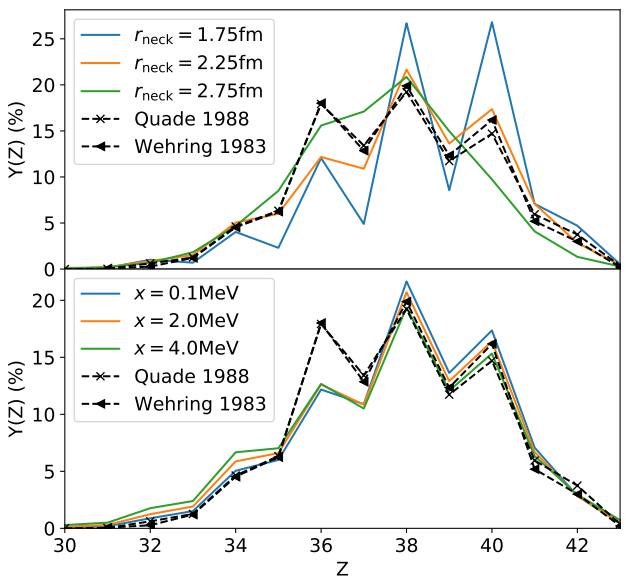

(a) Fragment charge yields obtained with our approach for the reaction ^{233}U($n_{\text{th.}}$,f) at $x = 0.1$ MeV with different neck radii (top panel) and with $r_{\text{neck}} = 2.25$ fm at different excitation energies (bottom panel). Our results are compared with experimental data with thermal incident neutron energies ($E_{\text{neut.}} = 0.0253$ eV) from [86, 87].

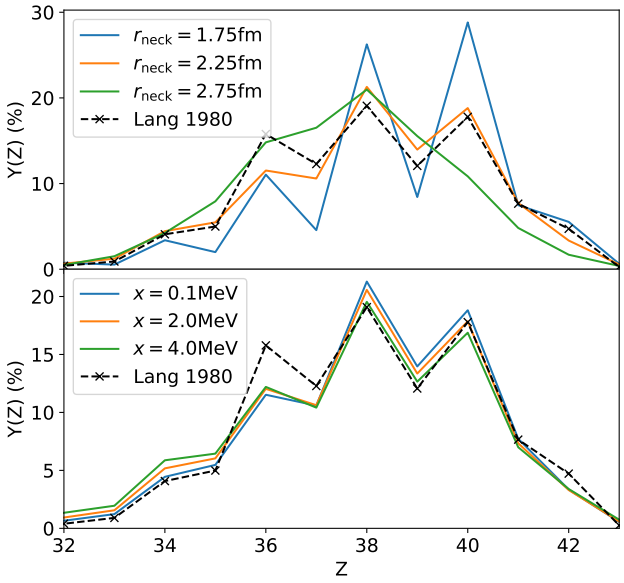

(b) Fragment charge yields obtained with our approach for the reaction ^{235}U($n_{\text{th.}}$,f) at $x = 0.1$ MeV with different neck conditions (top panel) and with $r_{\text{neck}} = 2.25$ fm at different excitation energies (bottom panel). Our results are compared with experimental data with thermal incident neutron energies ($E_{\text{neut.}} = 0.0253$ eV) from [86, 87].

A. Results

We have used our approach to calculate the fission fragment charge and mass probability distribution before prompt emission for the reactions ^{233}U(n,f) and ^{235}U(n,f). In Figs. 2a and 2b we highlight the charge yields of these reactions respectively. The upper panels of Fig. 2a and Fig. 2b show an important variation of the yields according to the definition of the scission line for both reactions. This behavior is due to the minimization of the energy to obtain our microscopic states [52]. The lower panels of Fig. 2a and Fig. 2b exhibit very little variation of our charge yields according to the excitation energy in the range $0.1 - 4.0$ MeV above the fission barrier. At $r_{\text{neck}} = 2.25$ fm, our charge yields present a very good quantitative agreement with experimental data for nearly all proton numbers.

As previously mentioned, our approach enables the determination of the mass and charge yields $Y(Z, A)$. Our charge yields for different fixed fragment masses are presented in Fig. 3 for the reaction ^{233}U(n,f) and ^{235}U(n,f). Our independent yields (solid orange lines) are obtained by assuming that the prompt neutron emission multiplicity distribution, P_n, depends on the mass of the fragments only. To estimate it, we first fit the parameter p of the probability mass function of the binomial random variable $\mathcal{B}(N = 5, p)$ on experimental data from Ref. [88] as suggested in [89]. We then shift the distribution for each fragment mass such that the expected value is equal to $\bar{\nu}(A)$ from Refs. [90, 91] to obtain $P_n(A)$. Finally, the pre-neutron yields are corrected according to $P_n(A)$ to obtain our estimation of independent yields. This method is easy to implement and fast, albeit simple; providing a means for comparison with experimental independent yield data. The presented theoretical yields correspond to $x = 0.1$ MeV. We note that the difference between each isobaric charge yields at different excitation energy were too small to distinguish them, and therefore were not included in these two figures.

Finally, Fig. 4 presents the full fragment mass and charge distribution we have obtained using our approach for the reactions ^{233}U($n_{\text{th.}}$,f) and ^{235}U($n_{\text{th.}}$,f), where the neck condition is $r_{\text{neck}} = 2.25$ fm. The main feature in these results is the reproduction of the charge polarization of the fragments. To estimate the charge polarization of the fragments, we have first calculated the average number of protons for each mass. Then, we have linearly fit it for the light- and heavy-fragments on all masses associated with a probability greater than 1%. The result of the fit is the upper blue lines for the light fragment and the lower ones for the heavy fragment. In each case, the expression of the linear curve is

$$Z_{\text{f}}^{\text{L}} = \eta_L A + s_L \tag{60}$$

$$Z_{\text{f}}^{\text{H}} = \eta_H A + s_H, \tag{61}$$

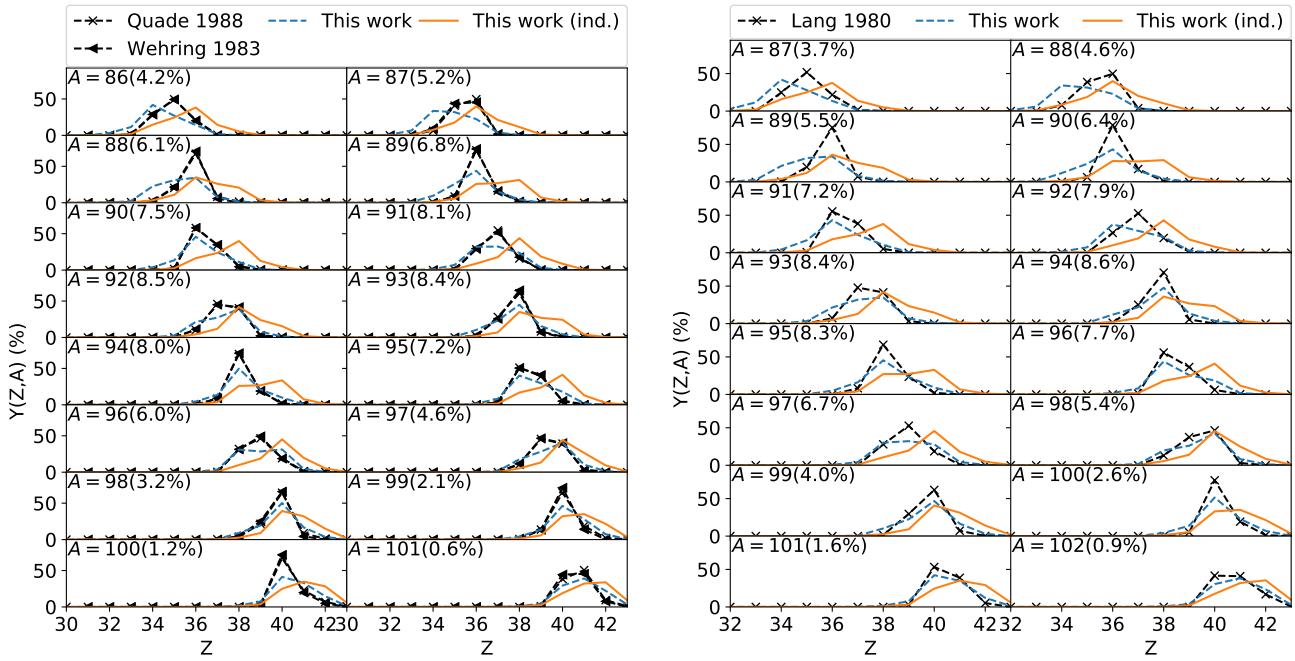

FIG. 3: Isobaric fragment charge yields (dashed blue lines) and the independent charge yields (solid orange lines), after prompt neutron emission, obtained with our approach for the reactions ^{233}U($n_{\rm th.}$,f) (left panel) and ^{235}U($n_{\rm th.}$,f) (right panel) with a neck condition $z_{\rm neck} = 2.25$ fm and an excitation energy above the barrier of $x = 0.1$ fm. Each curve is normalized at the fixed A to 100% and the fragment probability associated with each of the masses is listed in parentheses. We compare our results with experimental independent yields (dashed black curve) from Refs. [86, 87, 92].

where $Z_{\rm f}^{\rm L/H}$ is the charge of the light/heavy fragment. Since we only consider binary fission, $\eta_L = \eta_H \equiv \eta$. If the UCD assumption is satisfied (recall $\eta = \frac{Z}{A}$) then $\eta \approx 0.3932$ for the reaction ^{233}U(n,f) and $\eta \approx 0.3898$ for ^{235}U(n,f). However, the values of s_L and s_H are equal only if the UCD assumption is correct and the mass and charge distributions of the light- and heavy-fragments are aligned. Therefore, we introduce the quantity $\Delta_Z = s_L - s_H$, which measures the charge alignment and vanishes if the UCD is verified. The Δ_Z values, along with the one of η, s_L and s_H for each excitation energy x are reported in Table II for the reaction ^{233}U($n_{\rm th.}$,f) and Table II for the reaction ^{235}U($n_{\rm th.}$,f). For these two reactions, our approach indicates the light and heavy fragments distributions are misaligned by $\Delta_Z > 3.5$ charge units.

B. Validity of the convergence criteria

To analyze the convergence properties of our new algorithm, we calculate the probability distributions of the scission configurations $a_{\mathcal{S}}^{n}(\boldsymbol{q})$ for all steps, $n \leq n_{\rm max} = 150,000$, for the reaction ^{233}U(n,f). From this calculations, we can

	^{233}U(n,f)				^{235}U(n,f)			
x (MeV)	η	s_L	s_H	Δ_Z	η	s_L	s_H	Δ_Z
0.1	0.4338	-2.755	-6.763	4.007	0.4348	-3.312	-7.293	3.982
2.0	0.4299	-2.387	-6.216	3.829	0.4317	-3.015	-6.864	3.850
4.0	0.4230	-1.731	-5.240	3.509	0.4293	-2.788	-6.523	3.735

TABLE II: Characteristics of the charge alignment between the light- and heavy- fragment distributions for the reactions ^{233}U(n,f) and ^{235}U(n,f) represented by the blue curves of Fig. 4. If the UCD is verified, $\eta \approx 0.3932$ for ^{233}U(n,f), $\eta \approx 0.3898$ for ^{235}U(n,f), and $\Delta_Z = 0$.

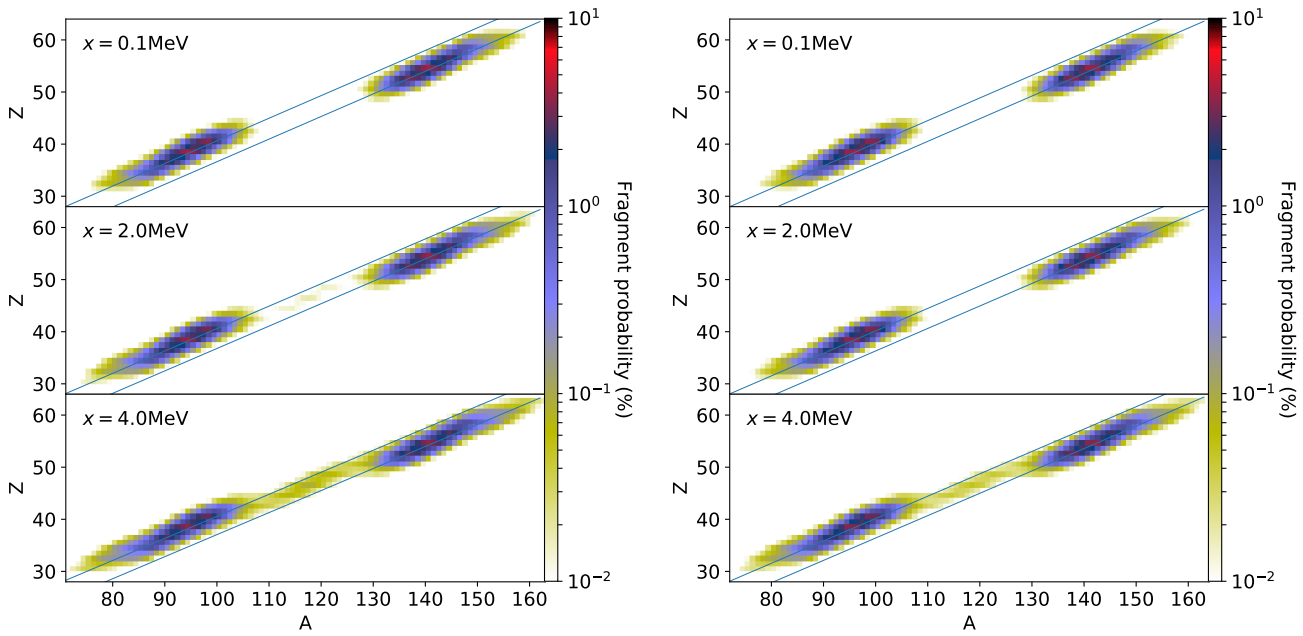

FIG. 4: Fragment mass and charge yields, before prompt neutron emission, obtained with our approach for the reactions ^{233}U($n_{\text{th.}}$,f) (left panel) and ^{235}U($n_{\text{th.}}$,f) (right panel) with a neck condition $z_{\text{neck}} = 2.25$ fm. Each panel shows the yield with different excitation energies above the barrier.

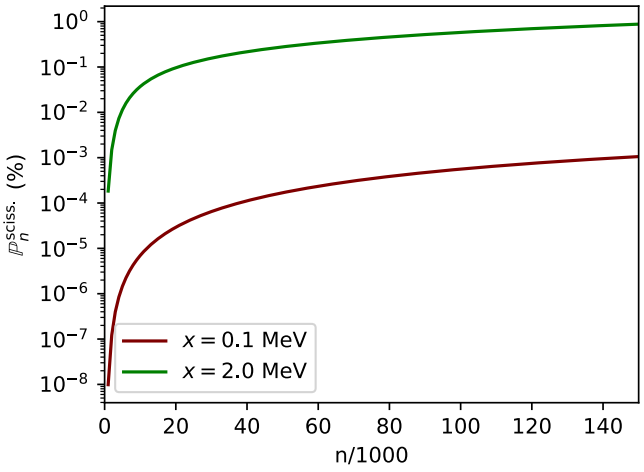

(a) Evolution of the scission probability according to the number of DPS iterations for the reaction ^{233}U(n,f).

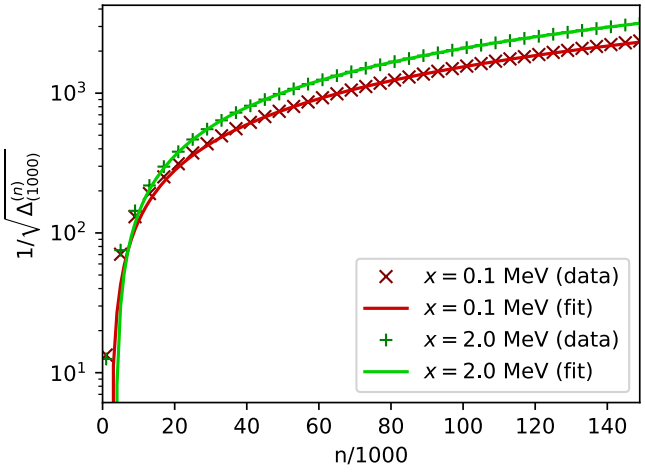

(b) Inverse-square-root of the evolution of the distance between successive probability distributions of the scission configurations for the reaction ^{233}U(n,f). To keep a readable graph, we have displayed only one point over four. A linear fit of the data is presented for comparison purposes.

extract the probability to reach scission after n iterations

$$\mathbb{P}_n^{\text{sciss.}} = \sum_{\boldsymbol{q}} \bar{a}_{\mathcal{R}}^{(n)}(\boldsymbol{q}) \ . \tag{62}$$

The evolution of this quantity with increasing n is shown in Fig. 5a. As expected, the lower excitation energy (red curve) is significantly below the run with higher excitation energy (green curve). For the same range of iterations, the evolution of the inverse-square-root of $\Delta_{(1000)}^{(n)}$ is presented in Fig. 5b. Recall that $\Delta_j^{(n)}$ is the convergence error given by Eq. (36).

The inverse-quadratic regime for $\Delta^{(n)}_{(1000)}$ is reached around $n \approx 20,000$ iterations where the ratio of paths that are reaching scission is $3.0 \times 10^{-5}\%$ for $x = 0.1$ MeV and $9.6 \times 10^{-2}\%$ for $x = 2.0$ MeV. In fact, the convergence seems to be at least quadratic, meaning that our convergence criteria is overestimating the error.

To further validate our convergence criteria, $\varepsilon^{(n,1000)}_{\text{eff.}}$, we have estimated it through a fit on the data applicable in the range of iterations $n_0, \ldots, n_1$. We compare our convergence criteria against data through the calculation of the relative error of the convergence criteria using $j = 1000$

$$D_{n_0,n_1} = \frac{\left[\varepsilon^{(n_0,j)}_{\text{eff.}}\Big|^{n_1}_{n_0} - \varepsilon^{(n_{\max}+1,j)}_{\text{eff.}}\Big|^{n_1}_{n_0}\right] - \sum_{k=0}^{\frac{n_{\max}-n_0}{j}} \Delta^{(n_0+jk)}_{(j)}}{\varepsilon^{(n_0,j)}_{\text{eff.}}\Big|^{n_1}_{n_0} - \varepsilon^{(n_{\max}+1,j)}_{\text{eff.}}\Big|^{n_1}_{n_0}}, \tag{63}$$

where $\varepsilon^{(n,j)}_{\text{eff.}}\Big|^{n_1}_{n_0}$ corresponds to the estimation of our convergence criteria using a fit between n_0 and n_1. The evolution of D_{n_0,n_1} according to the range used for the fit is presented Fig. 6 for which $n_0 > 5,000$ and $n_1 - n_0 \geq 5,000$. The relative error D_{n_0,n_1} associated with our convergence criteria between the iterations n_0 and n_1 is below 2% after only 10,000 iterations in both cases. D_{n_0,n_1} is greater than 0 almost everywhere, which means that our criteria slightly overestimates the convergence error.

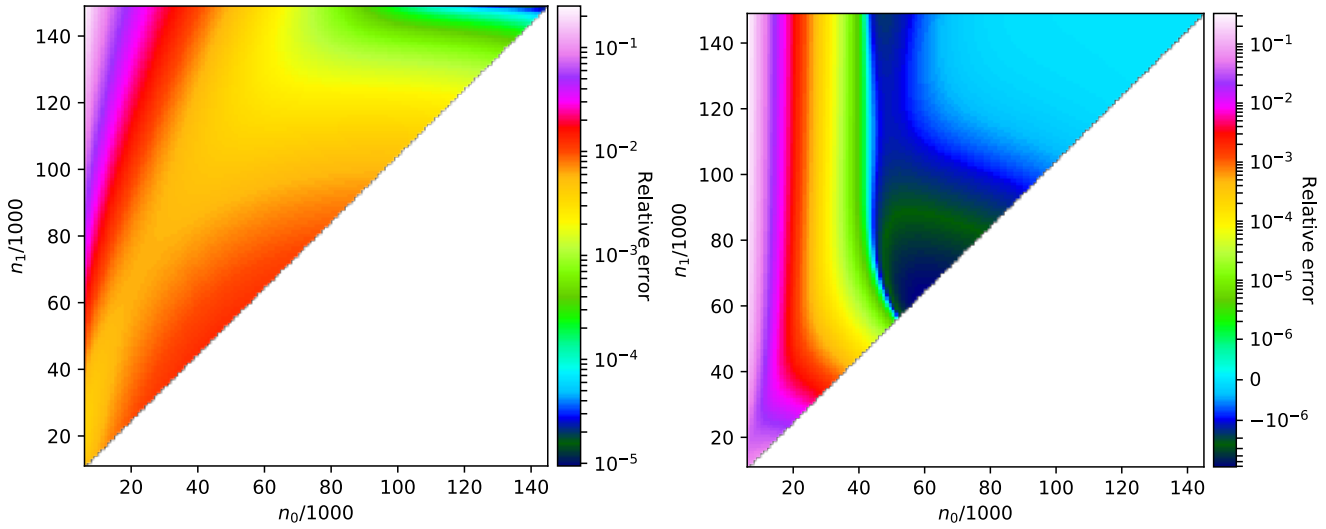

FIG. 6: Relative error D_{n_0,n_1}, defined by Eq. (63), between our convergence criteria and the exact convergence error, for each interval $n_0, \ldots, n_1$ of fitted data, for the reaction ^{233}U(n,f) at an excitation energy above the barrier of $x = 0.1$ MeV (left panel) and $x = 2.0$ MeV (right panel).

C. Comparison with the Metropolis implementation

We compare our new calculations to past work in order to show that we can reproduce these efforts within the context of our more general methodology. We use the implementation of a discrete random walk (DRW) as in Ref. [50] as the baseline FRLDM mass yield calculations. We perform these calculations for the reaction ^{233}U(n,f) at an excitation energy of $x \approx 4$ MeV above the barrier; noting that this value takes into account differences between the potential energy surface used in Ref. [50] and the potential energy surface of this work. The starting point of the DRW calculation is the ground state as chosen by the procedure of Ref. [50]. The biased potential is set to zero in the DRW calculation and we set the scission neck radius to be 2.25 fm. We accumulate 100,000 scission configurations for this comparison. With these parameters, we have nearly identical inputs as our new results shown in Sec. III A.

While the older mass yields rely only on the mass asymmetry coordinate, α_g, it is not sufficient to compare only this variable at scission as there could be changes in the distribution of other coordinates. Figure 7a shows the distribution of the scission configurations in the full collective coordinate lattice space, (i, j, k, l, n), between the standard random walk method and the method presented in this work. Despite the differences of the two approaches, exceedingly good

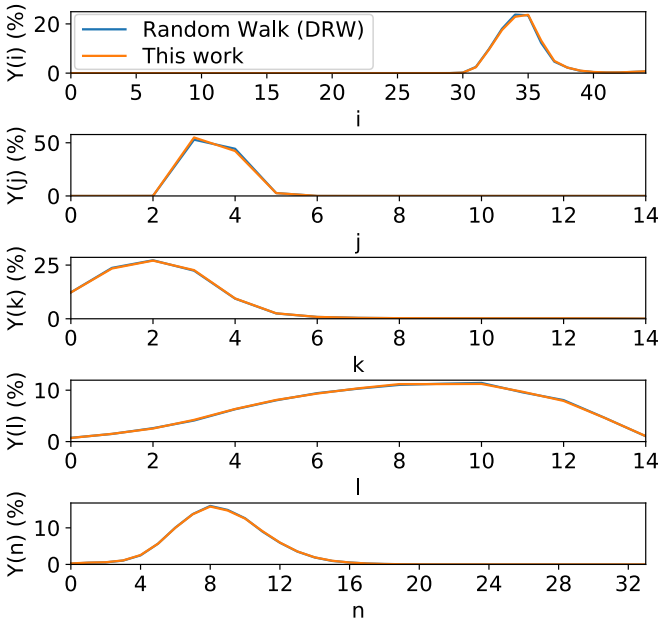

(a) Probability distributions to obtain a scission configuration associated with each integer indices (i, j, k, l, n) as defined in [63] estimated with state-of-the-art random walk with the code DRW (blue) and with this work (orange).

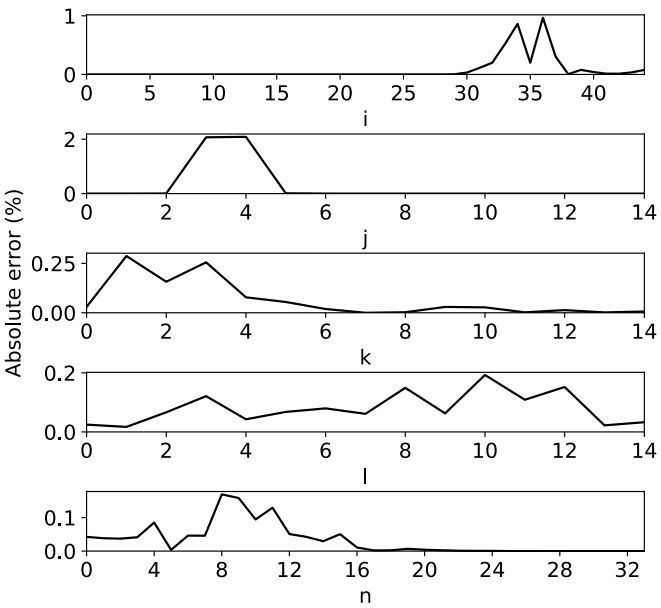

(b) Absolute error between the probability distributions presented in Fig. 7a.

agreement is found between the two algorithms. The absolute error between the two approaches is shown in Fig. 7b. We find that the statistical nature of the DRW algorithm leads to a maximum of $\sim 2\%$ error in the distribution of the scission neck radius, while the statistical error in α_g is the lowest of all the coordinates, on the order of .1%. These two figures show that we are successfully able to reproduce past work with our new technique and that older works indeed have quantitatively very good estimates of the mass yields within the context of FRLDM so long as a large number of scission events are calculated.

IV. CONCLUSION

With this work, we have improved the quality and predictive power of the mac-mic method in several areas. First, we have enhanced the quality of the nuclear PES by removing spurious continuum effects in our five-dimensional finite-range model. Further, our new resolution procedure of the Lipkin-Nogami equations enables the description of pairing effects with very high accuracy. Second, our new Deterministic-Probabilistic Algorithm (DPA) completely removes statistical uncertainties when computing the fission fragment distribution of a particular nucleus. DPA enables the starting point of our calculation to be located at the ground state (easily identifiable for all nuclei) without the requirement of including a biased potential that artificially tilts the PES. We have defined a high-accuracy convergence criterion associated with our algorithm that affords ability to monitor the error associated with the obtained results. Last, but not least, we have generalized the particle number projection technique introduced for independent quasi-particle states in Ref. [51, 78] and calculated scission configurations with it. This projection technique allows for the calculation of the coupled fragment charge and mass yield, $Y(Z, A)$. We refer to these improvements colloquially as the 'Enhanced Finite-Range Liquid-Drop Model' or eFRLDM for short.

Our first eFRLDM results are presented for the pre-neutron fission fragments probability distributions of the reactions ^{233,235}U(n,f) at different excitation energies. Our method can reproduce the odd-even staggering in the charge yields as well as the charge polarization of the fragments without any additional free parameters in the model. We find that a charge misalignment exists between the light and heavy fragments for these two reactions on the order of $\Delta_Z > 3.5$ charge units. Our results show a remarkable quantitative agreement with experimental data for charge yields and isobaric charge yields. We further highlight the capacity to reproduce past work within the context of our new methodology.

Looking forward, our description of the temperature dependence of the PES is treated from a macroscopic perspective in this work. Since microscopic effects are relevant, especially at low incident energies, it might change the relative contribution of different saddles and impact our results. Also, in this work, we have focused primarily on

pre-neutron fragments yields. However, due to the timescale of prompt particle emission, there is no such experimental data to compare directly. Hence, we can only compare with post-neutron yields, which induces further assumptions and models. A next step in this latter direction is therefore to pursue simulating the de-excitation of the nascent fragments. Improvements can be made to the description of microscopic temperature dependence, for example, by including finite-temperature effects directly into the microscopic states at each point of the PES, and this will assist in addressing the excitation energy dependence of our yield predictions. Yet another planned improvement is to refit the parameters of the model to account for the changes in the size of the basis and Strutinsky method.

The eFRLDM developed in this work is an ideal tool for large-scale precision calculations of fission fragment distributions required to model a range of phenomena, especially in astrophysical scenarios where it is important to obtain both charge and mass yields simultaneously to determine the relative abundances of lighter species. In addition to upcoming model improvements, we plan to study the application of our yields in a series of future efforts.

ACKNOWLEDGMENTS

The authors would like to thank Nicolas Schunck for his advice, his careful reading of the manuscript and his helpful comments, as well as Patrick Talou, Jørgen Randrup, Toshihiko Kawano, Ionel Stetcu, Arnie Sierk, and Peter Möller for valuable discussions over the years.

M.V. and M.R.M. were supported by the US Department of Energy through the Los Alamos National Laboratory. Los Alamos National Laboratory is operated by Triad National Security, LLC, for the National Nuclear Security Administration of U.S. Department of Energy (Contract No. 89233218CNA000001). M.V. and M.R.M. were partly supported by the Fission In R-process Elements (FIRE) topical collaboration in nuclear theory, funded by the U.S. Department of Energy and through the Los Alamos Laboratory Directed Research & Development Exploratory Research project entitled "Low-energy fission dynamics". This work was partly performed under the auspices of the U.S Department of Energy by Lawrence Livermore National Laboratory under Contract DE-AC52-07NA27344.

Appendix A: Finite-Range Liquid Drop Model (FRLDM)

We group here the main formulas and parameters that define our model that we use to calculate the nuclear potential energy surface. The macroscopic liquid-drop energy for even-even nuclei is

$$\begin{aligned} E_{\rm mac}(\boldsymbol{q}) = & M_{\rm H}Z + M_{\rm n}N \\ & - a_{\rm v}(1-\kappa_{\rm v}I^2)A \\ & + a_{\rm s}(1-\kappa_{\rm s}I^2)B_1(\boldsymbol{q})A^{2/3} \\ & + a_0 A^0 B_{\rm W}(\boldsymbol{q}) \\ & + c_1 \frac{Z^2}{A^{1/3}} B_3(\boldsymbol{q}) \\ & - c_4 \frac{Z^{4/3}}{A^{1/3}} \\ & + f(k_{\rm f} r_{\rm p}) \frac{Z^2}{A} \\ & - c_{\rm a}(N-Z) \\ & + W|I|B_{\rm W}(\boldsymbol{q}) \\ & - a_{\rm el} Z^{2.39}. \end{aligned} \tag{A1}$$

In this expression, A, Z, N are respectively the number of nucleons, protons and neutrons and I is the relative neutron excess,

$$I = \frac{N-Z}{A}. \tag{A2}$$

We note the pairing term is zero for even-even nuclei, and thus does not appear in the formula.

We shift globally the energy the PES such that the energy of the spherical point is zero. In this case, only the shape-dependent terms contribute to the PES. There are four such terms in our approach:

1. the surface energy, calculated assuming a finite-range Yukawa-plus-exponential nuclear interaction with no folding [93],
2. the Coulomb term, defined with a Yukawa folding of the sharp macroscopic density [94],
3. the A_0 energy from Ref. [41],
4. the Wigner term from Ref. [41].

By setting

$$\boldsymbol{\sigma}_a = \frac{|\boldsymbol{r} - \boldsymbol{r}'|}{a} \tag{A3}$$

and letting V represent the sharp-macroscopic density, the shape-dependent energies are the relative surface energy associated with a Yukawa-plus-exponential finite-range two-body interaction,

$$B_1(\boldsymbol{q}) = -\frac{A^{-2/3}}{8\pi^2 {r_0}^2 a^4} \iint_{\mathrm{V}} [\boldsymbol{\sigma}_a - 2] \, \frac{e^{-\boldsymbol{\sigma}_a}}{\boldsymbol{\sigma}_a} \, \mathrm{d}\boldsymbol{r} \, \mathrm{d}\boldsymbol{r}' \ , \tag{A4}$$

the relative Coulomb energy of a folded-Yukawa macroscopic density,

$$B_3(\boldsymbol{q}) = \frac{15 A^{-5/3}}{32\pi^2 a_{\mathrm{den}} {r_0}^5} \iint_{\mathrm{V}} \frac{\mathrm{d}\boldsymbol{r} \, \mathrm{d}\boldsymbol{r}'}{\boldsymbol{\sigma}_{a_{\mathrm{den}}}} \left[1 - \left(1 + \frac{\boldsymbol{\sigma}_{a_{\mathrm{den}}}}{2} \right) e^{-\boldsymbol{\sigma}_{a_{\mathrm{den}}}} \right] \ , \tag{A5}$$

and the shape-dependency of the A_0 and Wigner terms is defined as

$$B_{\mathrm{W}}(\boldsymbol{q}) = \begin{cases} \left(1 - \frac{S_3}{S_1} \right)^2 a_{\mathrm{d}} + 1 & \text{if there is a neck} \\ 1 & \text{otherwise.} \end{cases} \tag{A6}$$

In the last expression, $S1$ is the area of the maximum cross section of the smaller one of the end bodies and $S3$ is the area of the geometric shape $\boldsymbol{q}$ at the neck location. The definition of B_{W} is slightly different than in Refs. [41, 50] where the condition is only relative to the MQS parameter, σ_2. However, $\sigma_2 < 0$ does not imply the presence of a neck, defined as the existence of a local minimum in the sharp macroscopic density along the z-axis. Defining l_1, l_2 and l_3 as the respective centers of the left, middle and right bodies of the MQS shape, in the case where $l_2 \leq l_1$ or $l_3 \leq l_2$, the shape cannot exhibit a neck whatever the sign of σ_2. In this situation, B_{W} defined as in older work is not continuous at $\sigma_2 = 0$. Our new definition prevents this situation.

The model parameters we have used for the calculation of the PES are often referred to as `FRLDM2002` which correspond to the model parameters introduced in Ref. [64] with additional corrections of Ref. [81]. We present here only the parameters having an influence on the shape-dependent terms of the PES. The values of the fundamental constants we have used are Table IV references the parameters associated with the macroscopic part of the energy,

Parameter	Value	Unit
e_2	1.4399764	MeV fm
m_{amu}	931.4943335	MeV/c^2
m_{nuc}	1.007970689	amu
m_{n}	1.008664891	amu
m_{p}	1.007276487	amu

TABLE III: Truncation of the fundamental constants.

taken from [64]. Table V reports the macroscopic parameters taken from [81].

The parameters associated with the potential $V(\boldsymbol{r}; \boldsymbol{q})$ defined in (2) are

Appendix B: Resolution of the Lipkin-Nogami equations

When using a seniority-pairing interaction, the Lipkin-Nogami equations associated with a valence space of N_{v} energy levels are the set of $2N_{\mathrm{v}} + 3$ nonlinear equations (9)-(13) with the same number of unknowns v_k, ϵ_k, Δ, λ

Parameter	Value	Unit
r_0	1.16	fm
a	0.68	fm
$a_{\rm den}$	0.70	fm
W	30.0	MeV

TABLE IV: Part of the macroscopic parameters used in our approach to describe the fission process from [64].

Parameter	Value	Unit
$a_{\rm d}$	0.9	
$a_{\rm s}$	21.33000	MeV
$\kappa_{\rm s}$	2.378	MeV
a_0	2.04000	MeV

TABLE V: Part of the macroscopic parameters used in our approach to describe the fission process from [81].

and λ_2. Some of these equations are associated with high-derivatives. To reduce the amplitude and the number of non-zeros derivatives, we substitute u_k, v_k and ϵ_k by the variable x_k and θ_k according to

$$u_k = \cos(\theta_i) \tag{B1}$$
$$v_k = \sin(\theta_i) \tag{B2}$$
$$x_k = \epsilon_k - \lambda. \tag{B3}$$

The Lipkin-Nogami equations can then be rewritten and reorganized as

$$\boldsymbol{F}(\boldsymbol{p}) = 0, \tag{B4}$$

where, setting $\bar{k} = k - L_{\rm min}$,

$$F_{2N_{\rm v}}(\boldsymbol{p}) = L_{\rm min} - N_{\rm pair} + \sum_{k=L_{\rm min}}^{L_{\rm max}} \sin^2(\theta_k) \tag{B5}$$
$$F_{2N_{\rm v}+2}(\boldsymbol{p}) = \left[\sum_{k=L_{\rm min}}^{L_{\rm max}} \frac{1}{\sqrt{{x_k}^2 + \Delta^2}}\right] - \frac{2}{G} \tag{B6}$$
$$F_{2\bar{k}+1}(\boldsymbol{p}) = \frac{1}{2}\left[1 - \frac{x_k}{\sqrt{{x_k}^2 + \Delta^2}}\right] - \sin(\theta_k)^2 \tag{B7}$$
$$F_{2\bar{k}}(\boldsymbol{p}) = (4\lambda_2 - G)\sin(\theta_k)^2 + e_k - x_k - \lambda \tag{B8}$$
$$F_{2N_{\rm v}+1}(\boldsymbol{p}) = A(\boldsymbol{\theta})\lambda_2 - \frac{G}{4}B(\boldsymbol{\theta}), \tag{B9}$$

where the notations

$$A(\boldsymbol{\theta}) = \left[\sum_{k=L_{\rm min}}^{L_{\rm max}} \cos(\theta_k)^2 \sin(\theta_k)^2\right]^2 - \sum_{k=L_{\rm min}}^{L_{\rm max}} \cos(\theta_k)^4 \sin(\theta_k)^4 \tag{B10}$$

$$B(\boldsymbol{\theta}) = \left[\sum_{k=L_{\rm min}}^{L_{\rm max}} \cos(\theta_k)^3 \sin(\theta_k)\right] \times \left[\sum_{k=L_{\rm min}}^{L_{\rm max}} \cos(\theta_k) \sin(\theta_k)^3\right] - \sum_{k=L_{\rm min}}^{L_{\rm max}} \cos(\theta_k)^4 \sin(\theta_k)^4, \tag{B11}$$

and

$$\boldsymbol{p} = \Big(\theta_{L_{\rm min}}, x_{L_{\rm min}}, \ldots, \theta_{L_{\rm max}}, x_{L_{\rm max}}, \lambda, \lambda_2, \Delta\Big). \tag{B12}$$

The analysis of the dependencies of each equations leads to a maximum of $10N_{\rm v} + 2$ non-vanishing elements in the Jacobian matrix $J_{\boldsymbol{F}}(\boldsymbol{p})$. Also, $J_{\boldsymbol{F}}\boldsymbol{p}$ is *block-arrowhead*, which means that

$$J_{\boldsymbol{F}} = \begin{pmatrix} A & B \\ C & D \end{pmatrix}, \tag{B13}$$

Parameter	Value	Unit
$V_{\rm s}$	52.5	MeV
$V_{\rm a}$	48.7	MeV
$A_{\rm den}$	0.82	fm
$B_{\rm den}$	0.56	fm^2
$a_{\rm pot}$	0.8	fm
$k_{\rm p}$	0.025	
$l_{\rm p}$	28.0	
$k_{\rm n}$	0.01875	
$l_{\rm n}$	31.5	
a_1	15.677	MeV
a_2	22.00	MeV
J	35.0	MeV
L	99.0	MeV
Q	25.0	MeV
K	300.0	MeV

TABLE VI: Microscopic parameters associated with the potential (2).

where A is a block-diagonal matrix. In our case, the blocks of A are 2-dimensional matrices

$$A_{\bar{k}} = \begin{pmatrix} \frac{\partial F_{2\bar{k}}}{\partial \theta_k} & \frac{\partial F_{2\bar{k}}}{\partial x_k} \\ \frac{\partial F_{2\bar{k}+1}}{\partial \theta_k} & \frac{\partial F_{2\bar{k}+1}}{\partial x_k} \end{pmatrix}. \tag{B14}$$

The block-column matrix B and row-column matrix C are respectively associated with the following 2×3-dimensional and 3×2-dimensional blocks

$$B_{\bar{k}} = \begin{pmatrix} \frac{\partial F_{2\bar{k}}}{\partial \lambda} & \frac{\partial F_{2\bar{k}}}{\partial \lambda_2} & 0 \\ 0 & 0 & \frac{\partial F_{2\bar{k}+1}}{\partial \Delta} \end{pmatrix} \tag{B15}$$

$$C_{\bar{k}} = \begin{pmatrix} \frac{\partial F_{2N_{\rm v}}}{\partial \theta_k} & 0 \\ \frac{\partial F_{2N_{\rm v}+1}}{\partial \theta_k} & 0 \\ 0 & \frac{\partial F_{2N_{\rm v}+2}}{\partial x_k} \end{pmatrix}, \tag{B16}$$

In the following, we propose a method to solve the Lipkin-Nogami equations and more generally any system of equations associated with a *block-arrowhead* Jacobian matrix at each point $\boldsymbol{p}$ based on generalizations of the iterative Newton method. In our case, we use the cubic and the fifth-order iterative methods developed respectively by Homeier [95] and by Sharma & Gupta [82]. The idea of these methods is to improve the convergence properties of the Newton scheme by evaluating the Jacobian at different $\boldsymbol{p}$. For example, in the Sharpa & Gupta scheme, one step from iteration i to $i+1$ is

$$\boldsymbol{x}^{(i)} \leftarrow \boldsymbol{p}^{(i)} - \frac{1}{2} J_{\boldsymbol{F}}(\boldsymbol{p}^{(i)})^{-1} \boldsymbol{F}(\boldsymbol{p}^{(i)}) \tag{B17}$$

$$\boldsymbol{y}^{(i)} \leftarrow \boldsymbol{p}^{(i)} - J_{\boldsymbol{F}}(\boldsymbol{x}^{(i)})^{-1} \boldsymbol{F}(\boldsymbol{p}^{(i)}) \tag{B18}$$

$$\boldsymbol{p}^{(k+1)} \leftarrow \boldsymbol{y}^{(i)} - \Big[a J_{\boldsymbol{F}}(\boldsymbol{x}^{(i)})^{-1} + b J_{\boldsymbol{F}}(\boldsymbol{y}^{(i)})^{-1} \Big] \boldsymbol{F}(\boldsymbol{y}^{(i)}), \tag{B19}$$

where the fifth-order convergence is obtained when $a = 2$ and $b = -1$. The Newton scheme is recovered by doing only the first step and $\boldsymbol{p}^{(i+1)} \leftarrow \boldsymbol{x}^{(i)}$, while the two first steps are present in the Homeier scheme and $\boldsymbol{p}^{(i+1)} \leftarrow \boldsymbol{y}^{(i)}$.

The blockwise inversion theorem gives the inverse of the Jacobian matrix as

$$\boldsymbol{J}_{\boldsymbol{F}}(\boldsymbol{p})^{-1} = \begin{pmatrix} A^{-1} + IM & -IT^{-1} \\ -M & T^{-1} \end{pmatrix}, \tag{B20}$$

where

$$I = A^{-1} B \tag{B21}$$

$$T = D - CI \tag{B22}$$

$$M = T^{-1} C A^{-1}. \tag{B23}$$

Note that it is assumed that A and T are invertible. when it is not the case, we slightly perturb the diagonal elements of the non-invertible matrix. This method requires inversion of N_v 2-dimensional matrices $A_{\bar{k}}$ and one 3-dimensional matrix T. However, the procedure gives a dense matrix. Instead, we directly calculate the four vectors

$$\boldsymbol{a}^{(i)} = J_{\boldsymbol{F}}(\boldsymbol{p}^{(i)})^{-1}\boldsymbol{F}(\boldsymbol{p}^{(i)}) \tag{B24}$$

$$\boldsymbol{b}^{(i)} = J_{\boldsymbol{F}}(\boldsymbol{x}^{(i)})^{-1}\boldsymbol{F}(\boldsymbol{p}^{(i)}) \tag{B25}$$

$$\boldsymbol{c}^{(i)} = J_{\boldsymbol{F}}(\boldsymbol{x}^{(i)})^{-1}\boldsymbol{F}(\boldsymbol{y}^{(i)}) \tag{B26}$$

$$\boldsymbol{d}^{(i)} = J_{\boldsymbol{F}}(\boldsymbol{y}^{(i)})^{-1}\boldsymbol{F}(\boldsymbol{y}^{(i)}), \tag{B27}$$

such that

$$\boldsymbol{x}^{(i)} \leftarrow \boldsymbol{p}^{(i)} - \frac{1}{2}\boldsymbol{a}^{(i)} \tag{B28}$$

$$\boldsymbol{y}^{(i)} \leftarrow \boldsymbol{p}^{(i)} - \boldsymbol{b}^{(i)} \tag{B29}$$

$$\boldsymbol{p}^{(k+1)} \leftarrow \boldsymbol{y}^{(i)} - \left[a\boldsymbol{c}^{(i)} + b\boldsymbol{d}^{(i)}\right]. \tag{B30}$$

In the following, we note $\boldsymbol{e} = \boldsymbol{a}^{(i)}, \boldsymbol{b}^{(i)}, \boldsymbol{c}^{(i)}$ or $\boldsymbol{d}^{(i)}$ and $\boldsymbol{f} = \boldsymbol{F}(\boldsymbol{p}^{(i)})$ or $\boldsymbol{F}(\boldsymbol{p}^{(i)})$ according to the equation (B24)-(B27) considered. By injecting (B20) in (B24)-(B27) we obtain

$$\boldsymbol{e}_0 = A^{-1}\boldsymbol{f}_0 + IM\boldsymbol{f}_0 - IT^{-1}\boldsymbol{f}_1 \tag{B31}$$

$$\boldsymbol{e}_1 = -M\boldsymbol{f}_0 + T^{-1}\boldsymbol{f}_1, \tag{B32}$$

where

$$\boldsymbol{e} = \begin{pmatrix}\boldsymbol{e}_0\\ \boldsymbol{e}_1\end{pmatrix} \boldsymbol{f} = \begin{pmatrix}\boldsymbol{f}_0\\ \boldsymbol{f}_1\end{pmatrix}, \tag{B33}$$

and $\boldsymbol{e}_0$ and $\boldsymbol{f}_0$ are vectors of dimension $2N_\mathrm{v}$ and $\boldsymbol{e}_1$ and $\boldsymbol{f}_1$ are vectors of dimension 3. The expression of $\boldsymbol{e}_1$ appears in the expression of $\boldsymbol{e}_0$. Therefore, once $\boldsymbol{e}_1$ is obtained by using (B32), $\boldsymbol{e}_0$ can be obtained through the expression

$$\boldsymbol{e}_0 = A^{-1}\boldsymbol{f}_0 - I\boldsymbol{e}_1. \tag{B34}$$

Lastly, we note our convergence criteria is set to $\varepsilon^{\mathrm{LN}}(\boldsymbol{p}) < 10^{-10}$, where, using the aforementioned functions F_k,

$$\varepsilon^{\mathrm{LN}}(\boldsymbol{p}) = \max_k |F_k(\boldsymbol{p})| \ . \tag{B35}$$

[1] N. Tsoulfanidis and R. G. Cochran, Nuclear Technology **93**, 263 (1991).

[2] "Neutron chain fission reactors," in *Nuclear Reactor Physics* (John Wiley & Sons, Ltd, 2018) Chap. 2, pp. 33–42.

[3] R. C. Pardo, G. Savard, S. Baker, C. Davids, E. F. Moore, R. Vondrasek, and G. Zinkann, Nuclear Instruments and Methods in Physics Research B **261**, 965 (2007).

[4] J. Carlson, M. P. Carpenter, R. Casten, C. Elster, P. Fallon, A. Gade, C. Gross, G. Hagen, A. C. Hayes, D. W. Higinbotham, C. R. Howell, C. J. Horowitz, K. L. Jones, F. G. Kondev, S. Lapi, A. Macchiavelli, E. A. McCutchen, J. Natowitz, W. Nazarewicz, T. Papenbrock, S. Reddy, M. A. Riley, M. J. Savage, G. Savard, B. M. Sherrill, L. G. Sobotka, M. A. Stoyer, M. B. Tsang], K. Vetter, I. Wiedenhoever, A. H. Wuosmaa, and S. Yennello, Progress in Particle and Nuclear Physics **94**, 68 (2017).

[5] B. M. Sherrill, in *European Physical Journal Web of Conferences*, European Physical Journal Web of Conferences, Vol. 178 (2018) p. 01001.

[6] R. Surman and M. Mumpower, EPJ Web of Conferences **178** (2018), 10.1051/epjconf/201817804002.

[7] E. P. Abel, M. Avilov, V. Ayres, E. Birnbaum, G. Bollen, G. Bonito, T. Bredeweg, H. Clause, A. Couture, J. DeVore, M. Dietrich, P. Ellison, J. Engle, R. Ferrieri, J. Fitzsimmons, M. Friedman, D. Georgobiani, S. Graves, J. Greene, S. Lapi, C. S. Loveless, T. Mastren, C. Martinez-Gomez, S. McGuinness, W. Mittig, D. Morrissey, G. Peaslee, F. Pellemoine, J. D. Robertson, N. Scielzo, M. Scott, G. Severin, D. Shaughnessy, J. Shusterman, J. Singh, M. Stoyer, L. Sutherlin, A. Visser, and J. Wilkinson, Journal of Physics G: Nuclear and Particle Physics **46**, 100501 (2019).

[8] G. Mention, M. Fechner, T. Lasserre, T. A. Mueller, D. Lhuillier, M. Cribier, and A. Letourneau, Phys. Rev. D **83**, 073006 (2011).

[9] A. C. Hayes, J. L. Friar, G. T. Garvey, G. Jungman, and G. Jonkmans, Phys. Rev. Lett. **112**, 202501 (2014).

[10] M. Itkis, J. Aysto, S. Beghini, A. Bogachev, L. Corradi, O. Dorvaux, A. Gadea, G. Giardina, F. Hanappe, I. Itkis, M. Jandel, J. Kliman, S. Khlebnikov, G. Kniajeva, N. Kondratiev, E. Kozulin, L. Krupa, A. Latina, T. Materna, G. Montagnoli, Y. Oganessian, I. Pokrovsky, E. Prokhorova, N. Rowley, V. Rubchenya, A. Rusanov, R. Sagaidak, F. Scarlassara, A. Stefanini, L. Stuttge, S. Szilner, M. Trotta, W. Trzaska, D. Vakhtin, A. Vinodkumar, V. Voskressenski, and V. Zagrebaev, Nuclear Physics A **734**, 136 (2004).

[11] Y. Oganessian and V. Utyonkov, Nuclear Physics A **944**, 62 (2015), special Issue on Superheavy Elements.

[12] K. Godbey and A. S. Umar, Frontiers in Physics **8**, 40 (2020).

[13] C. Simenel, A. Wakhle, B. Avez, D. J. Hinde, R. du Rietz, M. Dasgupta, M. Evers, C. J. Lin, and D. H. Luong, in *European Physical Journal Web of Conferences*, European Physical Journal Web of Conferences, Vol. 38 (2012) p. 09001.

[14] G. Martínez-Pinedo, D. Mocelj, N. T. Zinner, A. Kelić, K. Langanke, I. Panov, B. Pfeiffer, T. Rauscher, K.-H. Schmidt, and F.-K. Thielemann, Progress in Particle and Nuclear Physics **59**, 199 (2007).

[15] S. Goriely, J.-L. Sida, J.-F. Lemaître, S. Panebianco, N. Dubray, S. Hilaire, A. Bauswein, and H.-T. Janka, Phys. Rev. Lett. **111**, 242502 (2013).

[16] M. Eichler, A. Arcones, A. Kelic, O. Korobkin, K. Langanke, T. Marketin, G. Martinez-Pinedo, I. Panov, T. Rauscher, S. Rosswog, *et al.*, The Astrophysical Journal **808**, 30 (2015).

[17] M. Mumpower, T. Kawano, T. Sprouse, N. Vassh, E. Holmbeck, R. Surman, and P. Möller, The Astrophysical Journal **869**, 14 (2018).

[18] N. Vassh, R. Vogt, R. Surman, J. Randrup, T. M. Sprouse, M. R. Mumpower, P. Jaffke, D. Shaw, E. M. Holmbeck, Y. Zhu, *et al.*, Journal of Physics G: Nuclear and Particle Physics **46**, 065202 (2019).

[19] N. Vassh, M. R. Mumpower, G. C. McLaughlin, T. M. Sprouse, and R. Surman, Astrophys. J. **896**, 28 (2020).

[20] P. Bonche, S. Koonin, and J. W. Negele, Phys. Rev. C **13**, 1226 (1976).

[21] Y. Engel, D. Brink, K. Goeke, S. Krieger, and D. Vautherin, Nuclear Physics A **249**, 215 (1975).

[22] R. Y. Cusson and H. W. Meldner, Phys. Rev. Lett. **42**, 694 (1979).

[23] S. Levit, J. W. Negele, and Z. Paltiel, Phys. Rev. C **22**, 1979 (1980).

[24] A. Bulgac, P. Magierski, K. J. Roche, and I. Stetcu, Phys. Rev. Lett. **116**, 122504 (2016).

[25] C. Simenel and A. S. Umar, Phys. Rev. C **89**, 031601(R) (2014).

[26] P. Goddard, P. Stevenson, and A. Rios, Phys. Rev. C **92**, 054610 (2015).

[27] C. Simenel and A. Umar, Progress in Particle and Nuclear Physics **103**, 19 (2018).

[28] Y. Tanimura, D. Lacroix, and S. Ayik, Phys. Rev. Lett. **118**, 152501 (2017).

[29] N. Schunck and L. M. Robledo, Reports on Progress in Physics **79**, 116301 (2016).

[30] J. Berger, M. Girod, and D. Gogny, Computer Physics Communications **63**, 365 (1991).

[31] H. Goutte, J. F. Berger, P. Casoli, and D. Gogny, Phys. Rev. C **71**, 024316 (2005).

[32] D. Regnier, N. Dubray, N. Schunck, and M. Verrière, Phys. Rev. C **93**, 054611 (2016).

[33] D. Regnier, N. Dubray, and N. Schunck, Phys. Rev. C **99**, 024611 (2019).

[34] W. Younes and D. Gogny, Phys. Rev. C **80**, 054313 (2009).

[35] W. Younes, D. M. Gogny, and J.-F. Berger, *A microscopic theory of fission dynamics based on the generator coordinate method*, Vol. 950 (Springer, 2019).

[36] J. Zhao, T. Nikšić, D. Vretenar, and S.-G. Zhou, Phys. Rev. C **99**, 014618 (2019).

[37] K.-H. Schmidt, B. Jurado, C. Amouroux, and C. Schmitt, Nuclear Data Sheets **131**, 107 (2016), special Issue on Nuclear Reaction Data.

[38] J.-F. Lemaître, S. Panebianco, J.-L. Sida, S. Hilaire, and S. Heinrich, Phys. Rev. C **92**, 034617 (2015).

[39] J.-F. Lemaître, S. Goriely, S. Hilaire, and J.-L. Sida, Phys. Rev. C **99**, 034612 (2019).

[40] P. Möller, W. D. Myers, H. Sagawa, and S. Yoshida, Phys. Rev. Lett. **108**, 052501 (2012).

[41] P. Mller, A. Sierk, T. Ichikawa, and H. Sagawa, Atomic Data and Nuclear Data Tables **109-110**, 1 (2016).

[42] V. M. Strutinsky, Nuclear Physics A **95**, 420 (1967).

[43] V. M. Strutinsky, Nuclear Physics A **122**, 1 (1968).

[44] M. BRACK, J. DAMGAARD, A. S. JENSEN, H. C. PAULI, V. M. STRUTINSKY, and C. Y. WONG, Rev. Mod. Phys. **44**, 320 (1972).

[45] T. Wada, N. Carjan, and Y. Abe, Nuclear Physics A **538**, 283 (1992).

[46] P. N. Nadtochy, A. Kelić, and K.-H. Schmidt, Phys. Rev. C **75**, 064614 (2007).

[47] A. J. Sierk, Phys. Rev. C **96**, 034603 (2017).

[48] J. Randrup and P. Möller, Phys. Rev. Lett. **106**, 132503 (2011).

[49] J. Randrup and P. Möller, Phys. Rev. C **88**, 064606 (2013).

[50] M. R. Mumpower, P. Jaffke, M. Verriere, and J. Randrup, Phys. Rev. C **101**, 054607 (2020).

[51] C. Simenel, Phys. Rev. Lett. **105**, 192701 (2010).

[52] M. Verriere, N. Schunck, and T. Kawano, Phys. Rev. C **100**, 024612 (2019).

[53] R. W. Hasse and W. D. Myers, *Geometrical relationships of macroscopic nuclear physics* (Springer Science & Business Media, 1988).

[54] A. V. Ramayya, J. H. Hamilton, J. K. Hwang, L. K. Peker, J. Kormicki, B. R. S. Babu, T. N. Ginter, A. Sandulescu, A. Florescu, F. Carstoiu, W. Greiner, G. M. Ter-Akopian, Y. T. Oganessian, A. V. Daniel, W. C. Ma, P. G. Varmette, J. O. Rasmussen, S. J. Asztalos, S. Y. Chu, K. E. Gregorich, A. O. Macchiavelli, R. W. Macleod, J. D. Cole, R. Aryaeinejad, K. Butler-Moore, M. W. Drigert, M. A. Stoyer, L. A. Bernstein, R. W. Lougheed, K. J. Moody, S. G. Prussin, S. J. Zhu, H. C. Griffin, and R. Donangelo, Phys. Rev. C **57**, 2370 (1998).

[55] A. V. Ramayya, J. K. Hwang, J. H. Hamilton, A. Sandulescu, A. Florescu, G. M. Ter-Akopian, A. V. Daniel, Y. T.

Oganessian, G. S. Popeko, W. Greiner, J. D. Cole, and GANDSCollaboration (GANDS95 Collaboration), Phys. Rev. Lett. **81**, 947 (1998).
[56] S. Vermote, C. Wagemans, O. Serot, J. Heyse, J. Van Gils, T. Soldner, and P. Geltenbort, Nuclear Physics A **806**, 1 (2008).
[57] S. Vermote, C. Wagemans, O. Serot, J. Heyse, J. Van Gils, T. Soldner, P. Geltenbort, I. AlMahamid, G. Tian, and L. Rao, Nuclear Physics A **837**, 176 (2010).
[58] F. Go *et al.*, Nuclear Physics A **734**, 213 (2004).
[59] J. Nix, *Further studies in the liquid-drop theory of nuclear fission*, Tech. Rep. LBNL Report #: UCRL-17958 (Lawrence Berkeley National Laboratory, 1968).
[60] J. R. Nix], Nuclear Physics A **130**, 241 (1969).
[61] J. R. Nix, Annual Review of Nuclear Science **22**, 65 (1972).
[62] M. Bolsterli, E. O. Fiset, J. R. Nix, and J. L. Norton, Phys. Rev. C **5**, 1050 (1972).
[63] P. Möller, A. J. Sierk, T. Ichikawa, A. Iwamoto, R. Bengtsson, H. Uhrenholt, and S. Åberg, Phys. Rev. C **79**, 064304 (2009).
[64] P. Moeller, J. R. Nix, W. D. Myers, and W. J. Swiatecki, Atomic Data and Nuclear Data Tables **59** (1995), 10.1006/adnd.1995.1002.
[65] A. Kruppa, Physics Letters B **431**, 237 (1998).
[66] N. Tajima, Y. R. Shimizu, and S. Takahara, Phys. Rev. C **82**, 034316 (2010).
[67] H. J. Lipkin, Annals of Physics **9**, 272 (1960).
[68] Y. Nogami, Phys. Rev. **134**, B313 (1964).
[69] D. G. Madland and J. Nix, Nuclear Physics A **476**, 1 (1988).
[70] J. Randrup, P. Möller, and A. J. Sierk, Phys. Rev. C **84**, 034613 (2011).
[71] P. Möller, J. Randrup, and A. J. Sierk, Phys. Rev. C **85**, 024306 (2012).
[72] P. Möller, J. Randrup, A. Iwamoto, and T. Ichikawa, Phys. Rev. C **90**, 014601 (2014).
[73] P. Möller and J. Randrup, Phys. Rev. C **91**, 044316 (2015).
[74] M. Caamaño, F. Rejmund, and K.-H. Schmidt, Journal of Physics G: Nuclear and Particle Physics **38**, 035101 (2011).
[75] A. C. Wahl, Los Alamos Report (2002), LA-13928.
[76] P. Möller and T. Ichikawa, The European Physical Journal A **51**, 1 (2015).
[77] M. Verriere and D. Regnier, Frontiers in Physics **8**, 233 (2020).
[78] G. Scamps, C. Simenel, and D. Lacroix, Phys. Rev. C **92**, 011602(R) (2015).
[79] D. Regnier, N. Dubray, M. Verriere, and N. Schunck, Computer Physics Communications **225**, 180 (2018).
[80] R. N. Perez, N. Schunck, R.-D. Lasseri, C. Zhang, and J. Sarich, Computer Physics Communications **220**, 363 (2017).
[81] P. Möller, A. J. Sierk, and A. Iwamoto, Phys. Rev. Lett. **92**, 072501 (2004).
[82] J. R. Sharma and P. Gupta, Computers & Mathematics with Applications **67**, 591 (2014).
[83] G. F. Bertsch and L. M. Robledo, Phys. Rev. Lett. **108**, 042505 (2012).
[84] L. M. Robledo, Phys. Rev. C **79**, 021302(R) (2009).
[85] V. Fomenko, Journal of Physics A: General Physics **3**, 8 (1970).
[86] U. Quade, K. Rudolph, S. Skorka, P. Armbruster, H.-G. Clerc, W. Lang, M. Mutterer, C. Schmitt, J. Theobald, F. Gnnenwein, J. Pannicke, H. Schrader, G. Siegert, and D. Engelhardt, Nuclear Physics A **487**, 1 (1988).
[87] B. W. Wehring, S. Lee, R. Strittmatter, and G. Swift, Trans. Am. Nucl. Soc.; (United States) **35** (1980).
[88] R. Gwin, R. Spencer, and R. Ingle, Nuclear Science and Engineering **87**, 381 (1984).
[89] B. C. Diven, H. C. Martin, R. F. Taschek, and J. Terrell, Phys. Rev. **101**, 1012 (1956).
[90] K. Nishio, M. Nakashima, I. Kimura, and Y. Nakagome, Journal of nuclear science and technology **35**, 631 (1998).
[91] K. Nishio, Y. Nakagome, H. Yamamoto, and I. Kimura, Nuclear Physics A **632**, 540 (1998).
[92] W. Lang, H.-G. Clerc, H. Wohlfarth, H. Schrader, and K.-H. Schmidt, Nuclear Physics A **345**, 34 (1980).
[93] H. J. Krappe, J. R. Nix, and A. J. Sierk, Phys. Rev. C **20**, 992 (1979).
[94] K. T. R. Davies and J. R. Nix, Phys. Rev. C **14**, 1977 (1976).
[95] H. Homeier, Journal of Computational and Applied Mathematics **169**, 161 (2004).